AD-A257 980

NAVAL POSTGRADUATE SCHOOL
Monterey, California

DTIC
ELECTE
DEC 14 1992
S E D

THESIS

FEASIBILITY STUDY OF IMPLEMENTING A
CODE DIVISION MULTIPLE ACCESS DATA LINK
UTILIZING FIBER OPTIC DELAY LINES

by

John W. Andre

September 1992

Thesis Advisor: John P. Powers

Approved for public release; distribution is unlimited.

92-31287

92 12 11 015

UNCLASSIFIED
SECURITY CLASSIFICATION OF THIS PAGE

REPORT DOCUMENTATION PAGE

Form Approved
OMB No. 0704-0188

1a. REPORT SECURITY CLASSIFICATION UNCLASSIFIED	1b. RESTRICTIVE MARKINGS
2a. SECURITY CLASSIFICATION AUTHORITY	3. DISTRIBUTION/AVAILABILITY OF REPORT Approved for public release; distribution is unlimited.
2b. DECLASSIFICATION/DOWNGRADING SCHEDULE	
4. PERFORMING ORGANIZATION REPORT NUMBER(S)	5. MONITORING ORGANIZATION REPORT NUMBER(S)
6a. NAME OF PERFORMING ORGANIZATION Naval Postgraduate School 6b. OFFICE SYMBOL (If applicable)	7a. NAME OF MONITORING ORGANIZATION Naval Postgraduate School
6c. ADDRESS (City, State, and ZIP Code) Monterey, CA 93943-5000	7b. ADDRESS (City, State, and ZIP Code) Monterey, CA 93943-5000
8a. NAME OF FUNDING/SPONSORING ORGANIZATION 8b. OFFICE SYMBOL (If applicable)	9. PROCUREMENT INSTRUMENT IDENTIFICATION NUMBER
8c. ADDRESS (City, State, and ZIP Code)	10. SOURCE OF FUNDING NUMBERS PROGRAM ELEMENT NO. / PROJECT NO. / TASK NO. / WORK UNIT ACCESSION NO.

11. TITLE (Include Security Classification)
Feasibility Study of Implementing Code Division Multiple Access Comm. Utilizing Fiber Optic Delay Lines

12. PERSONAL AUTHOR(S)
ANDRE, John W.

13a. TYPE OF REPORT	13b. TIME COVERED	14. DATE OF REPORT (Year,Month,Day)	15. PAGE COUNT
Master's Thesis	FROM _____ TO _____	September 1992	81

16. SUPPLEMENTARY NOTATION
The views expressed in this thesis are those of the author and do not reflect the official policy or position of the Department of Defense or the U.S. Government.

17. COSATI CODES			18. SUBJECT TERMS (Continue on reverse if necessary and identify by block number)
FIELD	GROUP	SUB-GROUP	CDMA, Fiber Optics, Multiple Access, Spread Spectruum, Delay Lines

19. ABSTRACT (Continue on reverse if necessary and identify by block number)

This thesis investigated the feasibility of implementing a code division multiple access (CDMA) data link that employs fiber-optic delay-line signal processing. A two-user unidirectional data link was built and tested. A review was done of the various coding techniques and signals as used in spread spectrum systems. The thesis discusses hardware design and component selection from both an overall system structure to a more detailed component design. Results of the overall design effort show that a CDMA scheme employing fiber-optic delay lines provides a viable option for multiple access networks supporting high rates of data transfer. Additionally the lack of network synchronization between transmitter and receiver makes this particular scheme straightforward to implement.

20. DISTRIBUTION/AVAILABILITY OF ABSTRACT	21. ABSTRACT SECURITY CLASSIFICATION	
[X] UNCLASSIFIED/UNLIMITED [ ] SAME AS RPT. [ ] DTIC USERS	UNCLASSIFIED	
22a. NAME OF RESPONSIBLE INDIVIDUAL POWERS, John P.	22b. TELEPHONE (Include Area Code) (408) 646 - 2679	22c. OFFICE SYMBOL EC/Po

DD Form 1473, JUN 86 Previous editions are obsolete. SECURITY CLASSIFICATION OF THIS PAGE
S/N 0102-LF-014-6603 Unclassified

Approved for public release; distribution is unlimited

Feasibility Study of Implementing a
Code Division Multiple Access Data Link
Utilizing Fiber Optic Delay Lines

by

John W. Andre
Lieutenant, United States Navy
B.S., Savannah State College, 1984

Submitted in partial fulfillment of the
requirements for the degree of

MASTER OF SCIENCE IN ELECTRICAL ENGINEERING

from the

NAVAL POSTGRADUATE SCHOOL
September 1992

Author: _____
John W. Andre

Approved By: _____
John P. Powers, Thesis Advisor

_____
Alex W. Lam, Second Reader

_____
Michael A. Morgan, Chairman,
Department of Electrical and Computer Engineering

ABSTRACT

This thesis investigated the feasibility of implementing a coded division multiple access (CDMA) data link that employs fiber-optic delay-line signal processing. A two-user unidirectional data link was built and tested. A review was done of the various coding techniques and signals as used in spread spectrum systems. The thesis discusses hardware design and component selection from both an overall system structure to a more detailed component design. Results of the overall design effort show that a CDMA scheme employing fiber optic delay lines provides a viable option for multiple access networks supporting high rates of data transfer. Additionally the lack of network synchronization between transmitter and receiver makes this particular scheme straightforward to implement.

Accesion For
NTIS CRA&I
DTIC TAB
Unannounced
Justification
By
Distribution /
Availability Codes
Dist | Avail and / or Special
A-1

TABLE OF CONTENTS

LIST OF TABLES

LIST OF FIGURES

I. INTRODUCTION

A. THE SPECTRUM AND NETWORKS

As communications theory and hardware technology continue to advance, the demand for communications services will continue grow. This growth will place new demands on the usable portion of the microwave and radio frequency spectrum. This increase in spectrum usage results in congestion and the situation is not expected to improve. Additional demands placed on the spectrum have been met administratively because technology has expanded the amount of the spectrum that is usable while at the same time decreasing the necessary bandwidth to support services. However, as advances in technology tend to level, the expected demand for new services will continue to rise. In the past, these events have forced spectrum administrators and engineers to consider alternative approaches to its efficient usage. To overcome these problems of congestion and demand, the techniques of spread spectrum have been advocated and implemented.

The same problems that have affected the microwave and radio frequency spectrum are also applicable to telecommunications and local area networks. However, the simple application of spread spectrum techniques to existing metallic cable networks is not a viable option. These techniques require more channel bandwidth than can be supported. What is more important is the issue of transmission data rate, which is also restricted by channel bandwidth. For reasons of bandwidth alone, industry is now upgrading

telecommunications networks by installing optical fiber as the network medium. Just as the transistor allowed for the application of spread spectrum techniques to commercial communications, optical fiber and components will also allow these principles to be applied to networks providing increased performance, diversity of services, and future expansion.

B. SPREAD SPECTRUM SIGNALS AND OPTICAL FIBER

Spread spectrum techniques have been successfully used in satellite communications and mobile-radio systems. The ability to spread narrowband information over a wide frequency band is the essence of spread spectrum systems. This spreading of signal energy, in some cases to an extent that it drops below thermal noise levels, offers several advantages over higher power narrowband transmission. These advantages include low probability of detection to an unintended receiver, high interference rejection, and simultaneous access over a common band. Just as performance objectives vary from application to application, so do the spread spectrum techniques that are applied. Additionally, the ability to apply these techniques, while maintaining high data rates with low probability of bit error, have made their use attractive to military applications.

Many different methods of exploiting spread spectrum properties have been developed. To be considered a spread spectrum system, a system must satisfy two criteria [Ref. 1: p. 404].

1. The bandwidth of the transmitted signal, $s(t)$, needs to be much greater than that of the original message signal, $m(t)$.

2. The relatively wide bandwidth of $s(t)$ must be caused by an independent modulating waveform, $c(t)$, called the spreading waveform or signal, which must be known by the receiver in order for detection to occur.

As a result, the complex envelope of the spread spectrum signal is a function of the message signal and the spreading waveform. Typically a product function, of the form $g(t) = g_m(t)g_c(t)$, is used to describe the complex envelope-generating function, where $g_m(t)$ and $g_c(t)$ are the usual types of modulation functions that generate AM, PM, and FM. [Ref. 1: p. 404]

Several other methods of wideband transmission are also in use but do not meet the above criteria; consequently, they are not considered spread spectrum.

1. Spread Spectrum Signals

Spread spectrum signals are classified by the type of mapping functions associated with $c(t)$. Some of the most common spread spectrum signals are *direct sequence* (DS), *frequency hopping* (FH), and *hybrid* which includes both of the above [Ref. 1: p. 405]. In this thesis the DS form of spread spectrum will be implemented. A brief description of each will help develop an understanding for further discussion.

a. Direct Sequence

Direct sequence systems are the best known and most widely used spread spectrum systems. This is attributed to their relative simplicity in that they do not require a high-speed, fast-settling frequency synthesizer. Instead the data-modulated waveform is modulated a second time using a wideband spreading signal $c(t)$. The spreading signal is chosen to have properties that facilitate demodulation by the intended receiver and

make demodulation by the unintended receiver as difficult as possible. If the bandwidth of the spreading signal is large relative to the data bandwidth, the spread spectrum signal is dominated by the spreading signal and is nearly independent of the data signal. Figure 1 is a simple *binary phase shift keying-direct sequence* (BPSK-DS) spread spectrum system. Demodulation is accomplished in part by remodulating with the spreading code appropriately delayed. This remodulation or correlation of the receiver signal with the delayed spreading waveform is called despreading and is critical in all spread spectrum systems.

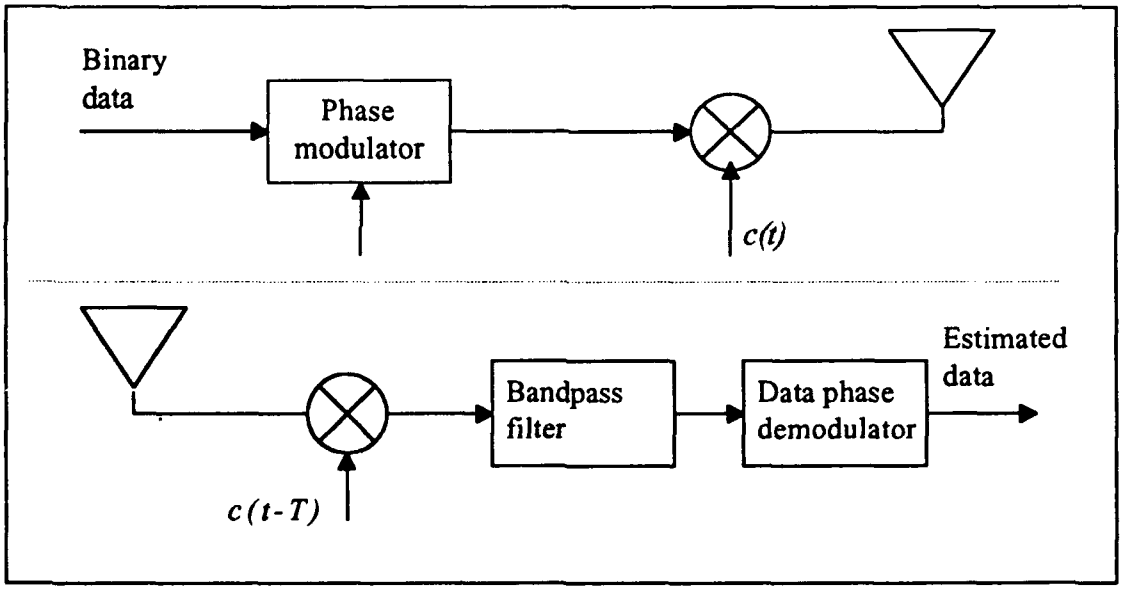

Figure 1. BPSK-DS spread spectrum transmitter (top) and receiver (bottom).
[After Ref. 2: p. 333]

Interference rejection is accomplished by the receiver despreading mixer, which spreads the spectrum of the interference at the same time the desired signal is despread. If the interference energy is spread over a bandwidth much larger than the data

bandwidth, most of the energy is rejected by the receiver's bandpass filter. [Ref. 2: p. 337]

b. Frequency Hopping

A second method for spreading the spectrum of a data-modulated carrier is to change the frequency of the carrier periodically. Frequency hopping systems are basically a form of *frequency shift keying* (FSK). The difference lies in the set of frequencies shifted to. Simple FSK uses two frequencies to signify a mark or a space. Frequency hoppers often have thousands of frequencies available. With the use of a frequency synthesizer, controlled by a coded sequence generator, the modulated carrier is sequentially hopped into a series of frequency slots into which the channel bandwidth has been partitioned [Ref. 3: p. 568]. The message signal now appears to be randomly spread over a wideband of frequencies. Identical equipment at the receiver, coordinated with a synchronizer, allows for recovery of the data signal.

c. Multiple Access Signals

Key to the discussion of DS and FH systems is their common use of a digital code sequence as the spreading waveform. If these sequences are designed properly, then multiple users can access the channel to make more efficient use of the spectrum. As such, we now have spread spectrum techniques associated with coded sequence multiple access, or more commonly known as *code division multiple access* (CDMA).

Frequency division multiple access (FDMA) and *time division multiple access* (TDMA) users are assigned different frequency slots or time slots, respectively. In CDMA all users share the same frequency space simultaneously in time. Although all three techniques provide a solution to the multiple access problem, studies have shown that FDMA and TDMA are more bandwidth efficient [Ref. 4: p. 14].

2. Optical Fiber

An inherent drawback in the use of these techniques on existing networks is the limited bandwidth available. The additional bandwidth required by spread spectrum can be accommodated by using a fiber optic channel and thus allowing spread spectrum techniques to be applied to networks. While fiber has been commercially available and successfully implemented for years, optical devices for broadband signal processing have not. As such, any signal processing of a transmitted signal must be done electrically. The process of optical-to-electrical and electrical-to-optical for signal processing greatly limits how much fiber bandwidth can be used. It, therefore, becomes desirable for an optical communications system to perform signal processing optically to exploit the tremendous potential fiber that holds as a transmission channel. [Ref. 5: p. 1601]

In some applications there is a need to consider signal transmission aspects such as antijam capabilities, interference rejection, and covert operations capability. All of these performance objectives can be achieved by using spread spectrum techniques with optical fiber channels. Optical fiber provides an excellent medium against electromagnetic interference (EMI) and electromagnetic pulse (EMP) effects. Consequently, the complex coding schemes used in traditional spread spectrum systems

for high security can be replaced by the inherent properties of optical fiber, making systems simpler and cheaper to implement.

THESIS OBJECTIVE

The objective of this thesis was to investigate the feasibility of implementing a *code division multiple access* scheme utilizing fiber optical delay lines for system encoding and decoding. A two-user unidirectional fiber-optic data link was designed and implemented supporting the highest possible data rate with the equipment available. Figure 2 shows a block diagram of the system. The digital circuits required at the transmitter and receiver interfaces for practical implementation will not be considered, nor will the design of any code sets. It was the optical encoding and decoding technique that was our primary interest. The goal of this initial effort was to establish the preliminary groundwork for future implementations which would support numerous users at higher data rates.

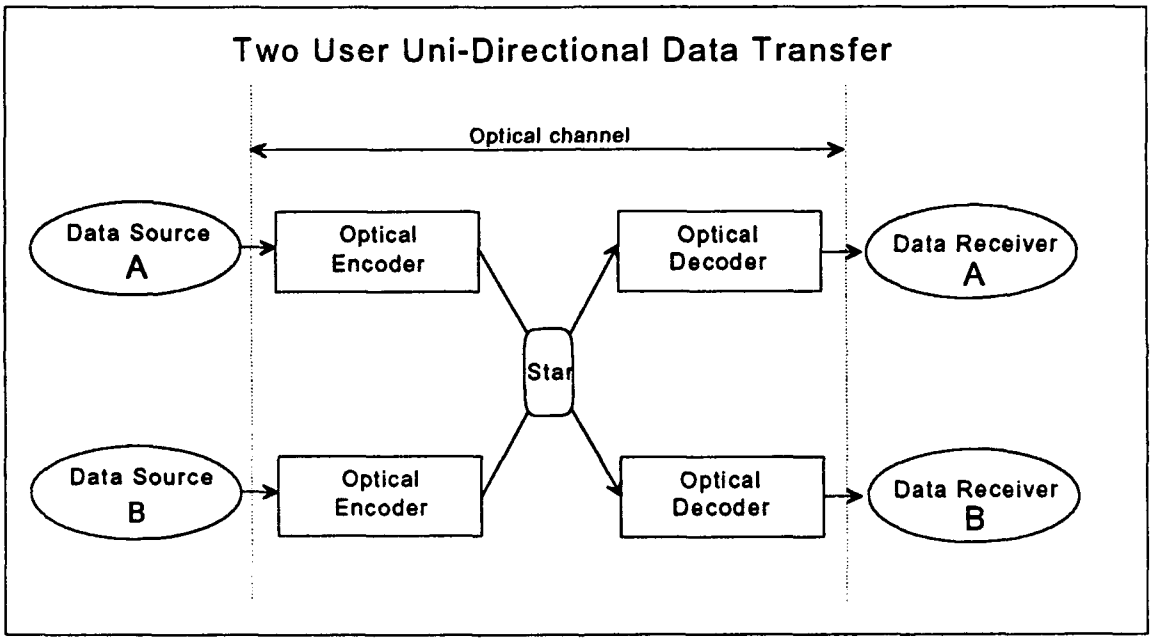

Figure 2. CDMA data link with optical encoding and decoding. [From Ref. 6: p. 824]

II. CDMA CODING

A. CDMA

CDMA is a spread spectrum technique that allows several different users to occupy the full bandwidth of the transmission channel simultaneously. Key to the success of any CDMA system is the choice of the specific codewords used to generate the spreading signals that provide orthogonal or near-orthogonal properties between each signal. Groups or *sets* of codewords must also be sufficiently large to accommodate the number of users that the system must support. Also, it is desirable that these codes be of optimum length such that they can be easily adapted to high-data-rate systems where speed, bandwidth, and security are all related to each other.

Spreading codes used to create the waveform *c(t)* are usually generated using a shift register. The shift register's output during each time interval T is some linear or nonlinear combination of the contents of the preceding time interval [Ref. 2: p. 365]. The spreading codes are all periodic sequences represented by "ones" and "zeros" with period N. It is convenient to represent a sequence of binary digits by a polynomial $b(D) = \cdots + b_{-2}D^{-2} + b_{-1}D^{-1} + b_0 + b_1D + b_2D^2 + \cdots$. The delay operator D is used to imply that the binary symbol, b_j, which multiplies D^j, occurs during the j^{th} time interval. Because the sequence is periodic, $b_n = b_{N+n}$ for any n. The spreading waveform derived from the spreading code is also periodic with period $T = NT_c$ and is specified by

$$c(t) = \sum_{n=-\infty}^{\infty} a_n p(t - nT_c) \ , \tag{1}$$

where $a_n = (-1)^{b_n}$ and *p(t)* is a unit pulse beginning at time zero and ending at time T_c [Ref. 2: p. 366]. The spreading waveform *c(t)* can be viewed as a bipolar representation of the "one" and "zero" code sequence. This form of the spreading code is more suitable as an input signal to a spreading modulator.

The spreading waveform *c(t)* is also deterministic, so the autocorrelation function can be defined by [Ref. 2: p. 366]

$$R_c(\tau) = \frac{1}{T}\int_0^T c(t)c(t+\tau)\,dt. \tag{2}$$

Since *c(t)* is periodic with period *T*, it follows that $R_c(\tau)$ is also periodic with period *T* [Ref. 2: p. 366].

Spreading waveforms are selected on a basis of certain desirable properties. For example, in traditional systems, the phase of the received spreading code $c(t-\tau)$ must initially be determined and tracked by the receiver. This is facilitated by choosing *c(t)* to have a autocorrelation function that is two-valued. When the system is used for multiple access, code sets must be found with good cross-correlation properties. When jamming

resistance is a concern, waveforms are used that have extremely long periods and are difficult for the jammer to generate. [Ref. 2: p. 365]

Once a signal has been spread, it is then sent over the channel whereupon each receiver demodulates and recovers their desired signal by despreading and filtering. This is accomplished by using an exact replica of the specific code sequence unique to that particular data signal. This despreading is nothing more than a correlation process.

B. CDMA SEQUENCES

1. PN Sequences

In CDMA, we stated that low-information rate electrical or optical signals are mapped using spreading codes to high rate electrical or optical sequences. These signals are normally of digital form and the spectrum of each transmitted digital signal is spread using a codeword that is unique to each user.

The ideal spreading code would be an infinite long sequence of equally likely random binary digits [Ref. 2: p. 366]. Unfortunately, the use of an infinite random sequence implies infinite storage in both the transmitter and the receiver. This is clearly not possible, so periodic codes, which exhibit noise-like properties, are always used. From the apparent randomness of the sequence, the name pseudorandom or pseudonoise (PN) sequence is derived. The time interval T that is used to transmit one data bit is subdivided into N equal time intervals called chips and is represented by T_c [Ref. 7: p. 376]. The duration of a codeword is equal to T and it follows that $T = NT_c$, where N is the number of chips in the sequence.

The PN sequence is then used to generate the randomly signed square wave, $c(t)$, having unit height with each square pulse being of duration T_c. This waveform is then multiplied with the data signal, thereby spreading the spectrum of the data signal by a factor of N. The effectiveness of interference rejection is directly proportional to the ratio of spread to unspread bandwidth, N, which is called the processing gain [Ref. 1: p. 410].

2. Conventional CDMA Sequences

Each data bit in a CDMA system is encoded into a waveform $s(t)$ that corresponds to a code sequence of N chips. This code sequence or codeword represents the destination address of the data bit. Each receiver, in turn, correlates its own code sequence with the received signal $s(t)$. The receiver output $r(t)$ can be represented by [Ref. 8: p. 547]

$$r(t) = \int_{-\infty}^{+\infty} s(z) f(z-t)\, dz \,, \tag{3}$$

where $f(t)$ represents the code sequence of the receiver.

If the signal arrives at the correct address, then $s(t) = f(t)$, and Equation 3 represents an autocorrelation function. If the signal has arrived at the wrong address, then $s(t) \neq f(t)$, and Equation 3 represents a cross-correlation function. [Ref. 8: p. 547]

In order to maximize the detection of a correct code word at the receiver in the presence of interference (other code words), two conditions must be met. First, the autocorrelation function must be maximized, and second, the cross-correlation functions must be minimized. These two conditions can be met by selecting code sets of orthogonal or near-orthogonal sequences. Two of the most popular code sets will be briefly discussed.

a. M-Sequences

The most widely known binary PN sequences are the maximal-length linear feedback shift-register sequences, or *m*-sequences [Ref. 3: p. 541]. These sequences have a period (length) of $N = 2^n - 1$, which is the longest sequence a *n*-stage binary shift register can generate. An important characteristic of a maximal length code is its discrete autocorrelation function which is two-valued and given by [Ref. 8: p. 548]:

$$r(t) = \begin{cases} N, & \text{for } t = 0 \\ -1, & \text{for } t = i\dfrac{T}{N}, \quad i = \pm 1; \pm 2, \cdots \end{cases} \tag{4}$$

where T is the data bit duration.

However, an undesirable characteristic of maximal length codes is that the peak of the cross-correlation function is not less than $-1 + 2^{(n+1)/2}$ [Ref. 8: p. 548]. This implies that certain sequences will interfere with one another and, thus, display multi-valued cross-correlation functions. Sequences that display only a three-valued

cross-correlation function are caller *preferred pairs* of *m*-sequences [Ref. 2: p. 405]. Since the set of preferred maximal length codes are few in number, maximal length codes are not suitable for CDMA applications where a large number of assignable addresses is required [Ref. 8: p. 548].

b. Gold Codes

Gold codes are families of codes with well-behaved cross-correlation properties. They are more suitable for CDMA because of the large number of orthogonal sequences available. Gold code sequences are generated by combining a pair of preferred maximal length sequences using modulo-2 addition, and, thus, exhibit many similar properties [Ref. 3: p. 544]. The autocorrelation function of a Gold sequence exhibits side lobes, depending on the pair of code sequences considered. The cross-correlation function is bounded. This implies that the maximum value of the peak of the cross correlation is equal to that of the original preferred maximal length sequences. [Ref. 8: p. 548]

Gold codes have been implemented with great success in many systems. They provide an answer to many of the limitations of m-sequences. However, Reference [6] provides a closer analysis of Gold code sequences and reveals some of the limitations of these codes that may prohibit their use in some applications.

For Gold codes, the *signal-to-noise ratio (SNR)* can be represented as the ratio of the square of the peak of the autocorrelation function to the variance of the amplitude of the interference. Assuming synchronization between the transmitter and the

receiver and considering other users' signals to be the dominant source of interference in the system, the *SNR* for Gold codes has been shown to be [Ref. 7: p. 123]:

$$SNR_{conventional} = 4\left[\frac{N^3}{(K-1)\left(N^2+N-1\right)}\right], \tag{5}$$

where K is the number of simultaneous users and N is the sequence length.

When K users are transmitting simultaneously, the total interference at a given receiver is the superposition of K–1 different cross-correlation functions. The variance of the total interference is the sum of the variances of the K–1 cross-correlation functions, which are assumed to be identical. Unfortunately, the variance of the amplitude of the cross-correlation function increases with both the number of users and the number of chips. The *SNR* for Gold codes is plotted versus K in Figure 3 for $N = 127$.

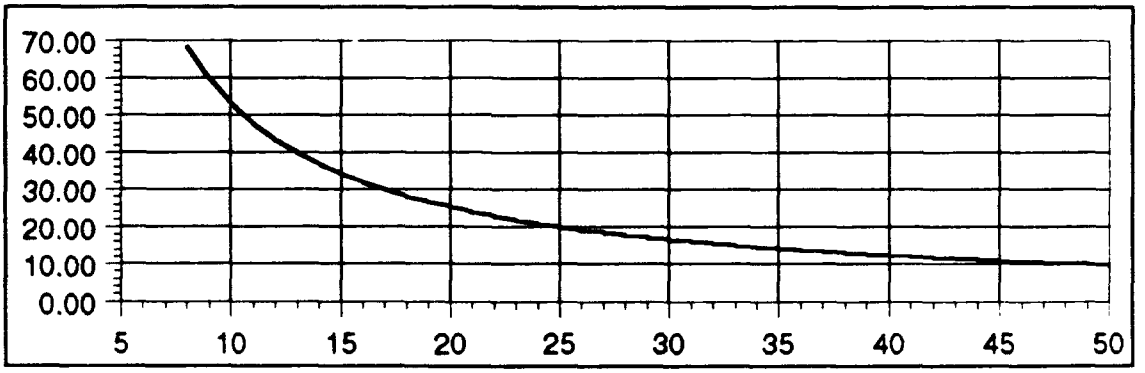

Figure 3. SNR for Gold codes ($N = 127$).

Clearly for a given number of chips per bit, the *SNR* decreases as the number of users increases. This implies that a lower *SNR* will yield a higher probability of bit error. Therefore, one disadvantage of Gold codes is apparent; to increase the number of simultaneous users while maintaining the same *SNR*, the number of chips per data bit must be increased. [Ref. 8: p. 549]

References [9] and [10] successfully implemented fiber-optic CDMA systems employing the coding schemes described above. Signal coding was accomplished using standard electronic components. A light source was then modulated with this signal and is transmitted over a optical fiber channel. The optical signal was converted back to a corresponding electric signal and decoded in a manner similar to that used in RF systems. Although this method of implementation is feasible, it is nevertheless limited by the processing speed of the electronics. Furthermore, if we consider the effects of increasing the number of chips per data bit or the number of users assigned, this type of system fails to take advantage of the available channel resources. An all-optical system, one that employs optical encoding and decoding, has the potential for increased number of chips per data bit and increased capacity over systems using electronic processing.

3. Optical Orthogonal Code Sequences (OOCs)

Before considering the application of spread spectrum techniques to an *all-optic* network, two important observations are worth noting.

First, it becomes apparent that increasing the processing speed, by using optical processing, allows an increase in *N*, and therefore an increase in the capacity of a CDMA system. However, a fundamental difference exists between optical processing and conventional processing, using, for example, optical delay lines [Ref. 11: p. 194]. Conventional (electronic) delay lines coherently combine tapped signals. The "1" and "0" chips of the code sequence can be manipulated to have a bipolar representation to facilitate correlation. Optical fiber delay lines, on the other hand, usually combine tapped signals incoherently, resulting simply in the summation of optical power. There is no negative component to be used in the correlation process. Though coherent optical processing is possible in principle, it is not practical at the present time, due to the high frequency of the optical carriers [Ref. 8: p. 549].

Secondly, using incoherent optical processing, the (1,0) levels of the transmitted optical code sequence correspond to light "ON" or light "OFF". For optical correlation, the peak of the autocorrelation function equals the number of 1's in the code sequence. The peak of the cross-correlation function equals the number of coincident 1's in all shifted versions of the two code sequences. For Gold codes, the number of 1's in each code sequence varies and, therefore, so does the peak of the autocorrelation function. The number of coincident 1's between shifted versions of the two code sequences can be large, therefore, so can the peak of the cross-correlation function. Gold code sequences are, therefore, not the optimum code choice for incoherent optical processing. [Ref. 8: p. 549]

A new set of code sequences is needed for CDMA applications employing optical processing. *Optical orthogonal codes* (OOCs) are related to but differ from other orthogonal codes and well-correlated sequences. The lack of "negative components" in an optical transmission data link dictates a different set of correlation properties. Most well correlated binary sequences are actually (+1,–1) sequences even though they use (1,0) notation. This is evident in the method used to calculate their correlations. They are intended for applications with both positive and negative signals available where the correlation constraint can be made zero. Furthermore, a well-correlated (+1,–1) sequence typically has about the same number of +1's and –1's while a good OOC has many more 0's than 1's in each codeword. This latter property of OOCs is very desirable in unipolar applications and will become apparent when we consider how the code sequence is generated. While each class of sequences can be used in the opposite application, the results are considered inferior. [Ref. 12: p. 596]

Another difference in the use of OOCs is that the codes can be calculated off-line and then applied to the CDMA system. This reduces system components and complexity and simplifies the implementation. Also, because incoherent detection is used, no synchronization is required between the transmitter and receiver. The correlation process is accomplished using a matched filter and data reconstruction is done using a threshold detector and a pulse generator. These properties of an all-optic implementation make realization relatively straight forward.

Reference 13 presents the results of a study to produce (1,0) sequences with good autocorrelation and cross-correlation properties. The best possible four- and

five-pulse sequences, supporting up to fifteen users, were found and presented in tabular form. References [5], [6], and [12] also give detailed accounts of alternate methods for generating sets of OOCs. While these methods are not considered unimportant, it is not the generation of codes that is the focus of this thesis but their implementation. For this thesis, codes presented in Reference 13 were used.

Because of the different methods used in the generation of code sets, notation tends to vary from reference to reference. For the remainder of this thesis, we will use the notation used in Reference 13. A brief description follows.

A code set is represented by $g(r,n)$, where r is the number of distinctive codes (users) in the set and n, which is called the sequence weight, is the number of "1's" in each sequence. Sequences are designated using vector notation. As an example, $\underline{X} = (x_1, x_2, x_3, \cdots x_L)$ and $\underline{Y} = (y_1, y_2, y_3, \cdots y_L)$ denote two sequences of length L. A pseudo-orthogonal (0,1) code set is one in which all members have autocorrelation and pairwise cross-correlations satisfying the following conditions:

Autocorrelation,

$$C_{xx}(t) = \begin{cases} n & t = 0 \\ \leq 1 & t \neq 0 \end{cases} \tag{6}$$

Cross-correlation,

$$C_{XY}(t) \leq 1 \quad \text{for all } t \tag{7}$$

Table 1 presents the codes for a two-user, weight four, sequence set. This set contains the actual codes used in this thesis. Numeric values under the set heading represent the pulse locations for the code sequences. The longest sequence of the two code set is designated "user 1" and is of length fourteen. As such, $L \geq 14$. Zero padding the sequences will have no effect on the sequence properties.

TABLE 1. SEQUENCE SOLUTION SET [After Ref. 13: Fig. 3].

Pulse Location For				
user	*g(2,4)*			
1	1	4	13	14
2	1	6	8	12

In Chapters 1 and 2 a brief introduction of spread spectrum signals, optical fiber, and coding techniques was given. Chapter 3 will focus on the system that was implemented. Initial considerations of the system design will be broken down into various parts for ease of discussion, each discussing the relative topics to this initial work.

III. SYSTEM OVERVIEW

A. DESIGN DESCRIPTION

We begin the design of the CDMA data link with a more detailed block diagram than was previously presented. Figure 2 has been expanded to reveal the delay lines used in the encoder and decoder and is shown in Figure 4. From Table 1, we used a code sequence whose weight is four, and thus, each encoder and decoder required four delay lines for optical processing. (The loops shown on each delay line are not to be confused with any real time-delay intervals but are used only to show each line's relative length.) As previously mentioned, we did not implement any of the circuitry required to recover usable data from the decoders. However, along with an optical detector, each receiver would contain a threshold detector and a pulse generator to complete the decoding process. In the sections to follow, descriptions of each of the data link components will be given. We will start with a broad system overview.

Each light source emits a narrow pulse into each encoder at the data rate. As this narrow pulse enters the first 1×4 splitter, it is divided into four pulses equal to one-fourth of the original amplitude (theoretically). The splitting process does not affect the pulse duration. The four pulses emerge from the first splitter and meet each of their respective delay lines. The delay lines delay each pulse the required number of delay units, generating the code sequence specified. The four pulses emerge from the delay lines, having undergone coupling and fiber attenuation, and enter the 4×1 splitter. The

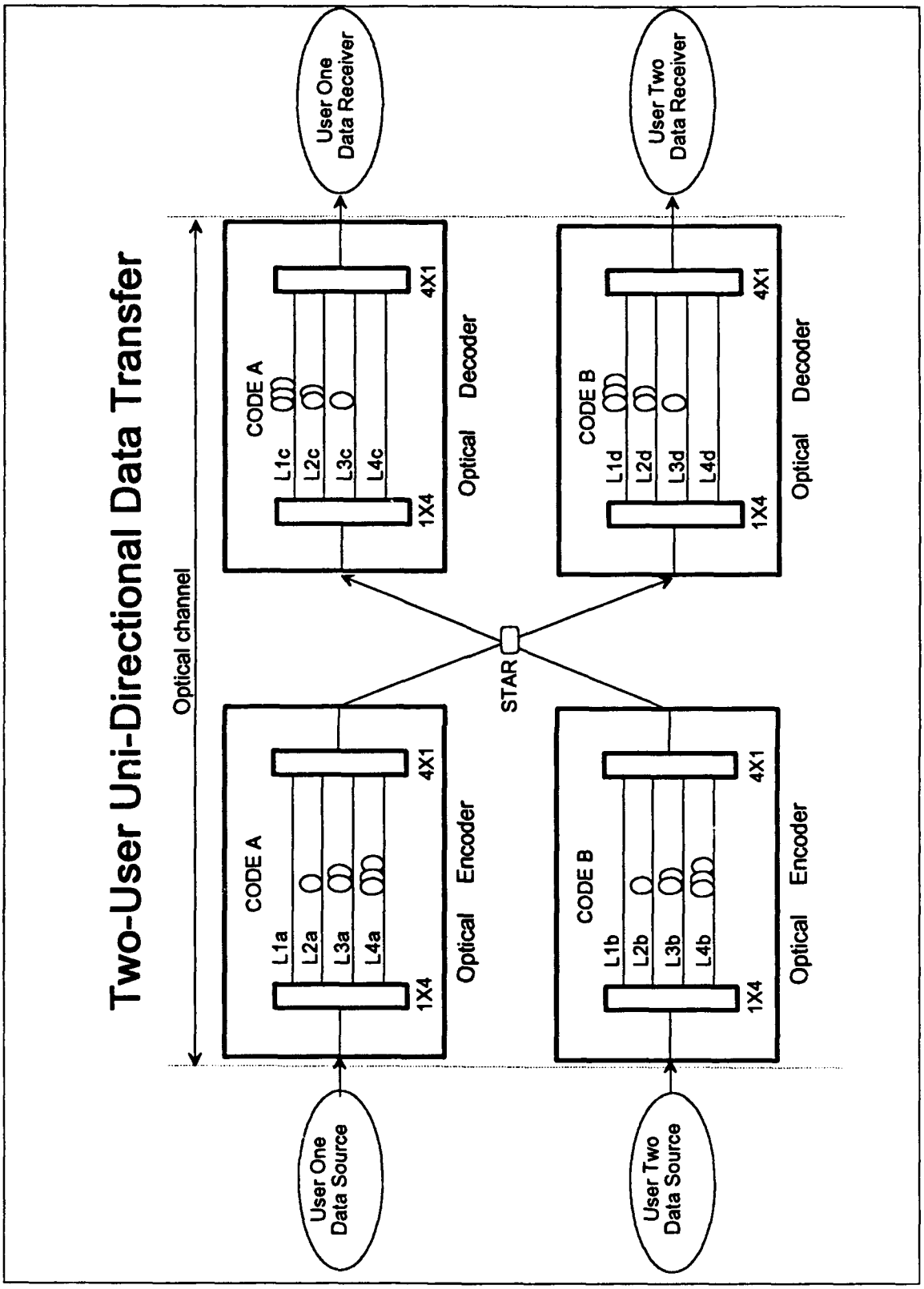

Figure 4. Two-User FO-CDMA data link.

4×1 splitter combines the four timed delayed pulses in a single fiber. One drawback with using a 4×1 splitter is that the pulses undergo another one-to-four reduction in amplitude. The four pulses now appear as a single optical sequence corresponding to the selected OOC.

The optical sequences then enter the 2×2 splitter (star) to be distributed to each receiver. The star is a unidirectional device, providing high cross-input rejection. On each of the output leads of the star, both of the input sequences appear with the same relative time spacing but reduced one-half in amplitude from their value on entering the star.

The input signal to either decoder can now be viewed as a sequence. The sequence is again split into four separate sequences by the decoder's 1×4 splitter and undergoes another one-to-four amplitude reduction. The sequences then continue down each of their respective delay lines and undergo additional attenuation. They are then recombined by the last 4×1 splitter and undergo another one-fourth reduction in amplitude. The key to the recombination process is the time delay that each of the decoder's delay lines provides. The delay lines are selected such that one of the four pulses of each of the four sequences are coincident temporally on the output lead of the splitter. To be more specific, the first pulse of the sequence that experiences the longest delayed arrives at the output of the 4×1 splitter the same instant in time as the last pulse of the sequence experiencing the shortest delay. Intermediate pulses of the intermediate sequences are delayed accordingly. The power of these coincident pulses of light adds and produce a large spike relative to the sums of other pulses in the sequences. The

relatively large spike corresponds to a data bit from the original input signal and would be used to trigger a threshold detector.

From the above description several points are worth noting:

1. The entire process of coding and decoding is done without the need of any synchronization between the transmitter and receiver.

2. The data link provides asynchronous communication access, free of any network control between users.

3. An apparent drawback is the high attenuation (loss) of the signal due to the numerous splitters and couplers.

B. INITIAL CONSIDERATIONS AND COMPONENT SELECTION

The initial layout of any communication system starts with a specification. A logical first step is to determine the number of users to support, and at what data rates. From the specification, the system's performance is clearly defined and design tradeoffs can be considered to meet the system's objective. For this thesis we made a broad initial specification to support two users at the highest possible data rate. In the following sections we will address component selection, system performance, and the hardware that was implemented. While most of the individual topics can be discussed with great detail, we will limit the scope of discussion to the pertinent points related to this thesis.

1. Bit Rate

One approach that could be used would be to determine the desired data rate, R_b, and then to proceed with the system's design to support this specification. Previously we stated that each data bit must be divided into a number of smaller time intervals called

chips. The length of the code sequence, L, determines the number of chips in the data bit time interval T. It follows that

$$T_c = T_b / L , \tag{8}$$

where T_b is the data bit period ($T_b = 1 / R_b$). From Table 1, we see that the length of the longest code sequence in the set is fourteen; therefore, each data bit must be divided into fourteen equal time slots. As an example, if R_b = 10 Mb/s, then T_b= 100 ns and $T_c = T_b / L$ = 7.14 ns.

This example was given to illustrate one important point. If the equipment available can not support a pulse width duration equal to T_c, then the desired data rate cannot be achieved. However, the above example can be worked in the reverse fashion. We determined that the equipment on hand could support T_c = 50 ns. This leads to R_b = 1.42 Mb/s. At this point, it is fair to assume that this is the maximum data rate that can be achieved with the present lab equipment and that any design adjustments can only reduce this rate.

2. Sources

For fiber optic systems, two types of sources are available, the light emitting diode (LED) and the laser diode. Either source can be found in both short and long wavelengths, typically around 850 nm and 1300 nm (or 1550 nm) respectively. The choice between the wavelength regions is based on several factors which include signal

dispersion, data rate, transmission distance, and cost. The spectral line width of a typical laser is much narrower than that of LED. This is important in the short wavelength region, where the spectral line width of a LED and the dispersion characteristics of silica fiber limit the data-rate-distance product to around 150 (Mb/s)•km [Ref. 14: p. 318]. For short link distances, the shorter wavelength devices may be suitable. However, if the transmission distance is relatively long, we may take advantage of the lower attenuation and dispersion that occurs within optical fiber at wavelengths around 1300 or 1550 nm. For higher data-rate-distance products (up to 2500 (Mb/s)•km) a laser must be used at short wavelengths. At the long wavelengths where signal dispersion is very low, data-rate-distance products of at least 1500 (Mb/s)•km are achievable with LEDs and values in excess of 25 (Gb/s)•km for lasers. [Ref. 14: p. 318]

Since laser diodes typically couple from 10 to 15 dB more optical power into a fiber than an LED, greater transmission distances are possible. This advantage and the lower dispersion properties of lasers may be offset by cost constraints. Not only are laser diodes more expensive than LEDs, but also laser transmitter circuits is more complex because the lasing threshold has to be dynamically controlled as a function of temperature and device aging. [Ref. 14: p. 318]

Another issue when selecting a source for a system of this type is the maximum possible modulation rate that the device is capable of achieving. At high modulation rates, inexpensive LEDs tend to have long rise and fall times producing irregular waveforms (non-square). On the other hand, laser diodes can provide very fast rise and

fall times, producing sharp square pulses more suitable for accurate chip placement in our coding application.

For this thesis it would appear that a quality LED source at short wavelengths would be suitable. However the main obstacle our link is not the dispersion properties of the fiber, but the high attenuation due to the numerous splitters used for signal processing. Ideally, a quality LED source could provide enough power and bandwidth for this particular application, but a laser would provide an extra margin of performance.

Figures 5 and 6 are waveforms of the two 1300 nm sources available for this thesis. These waveforms were captured with a Tektronix transient digitizer. Reference 15 provides a detailed description of its operation. A brief description of the symbols and measurements displayed with the waveform is given for clarity. Two cursors are displayed in the waveform window and their locations are represented with a "v" and inverted "v". A trigger position is also marked with a "T". Above the waveform window are measurements made with respect to these three symbols. V1, for example, is the voltage level associated with the first cursor (inverted "v") position. V2 is the voltage level associated with the second cursor ("v") position. The measured values "t1" and "t2" are the cursor's time positions relative to the trigger position "T". Values "DV" and "Dt" are the voltage and time difference between the cursors, respectively. In the lower portion of the waveform window are additional symbols. The record number, indicated by R1, identifies the currently displayed record. A time stamp, indicated by "0S", indicates the trigger point time on the currently displayed record, relative to the trigger point of the record #1 acquisition. Record 1 (R1) is always 0 [Ref. 15: p. 3-29]. The

record bar (lower right banded area) provides as approximate location of the current display, the trigger event, and the cursor locations relative to the entire digitized record. Channel status, displayed to the left of the waveform window, indicates the source channel, input range, offset, and vertical expansion factor. The small ground symbol is used to indicate the zero volts level.

The waveform displayed in Figure 5 was produced using a Photodyne 7250XR laser pulse generator with a long (50 ns) pulse selected. The waveform displayed in Figure 6 was produced with a Photodyne 7750XR LED optical signal generator being modulated by an external 50 ns pulse. We note that the LED source does not provide the clean sharp edges that the laser produces.

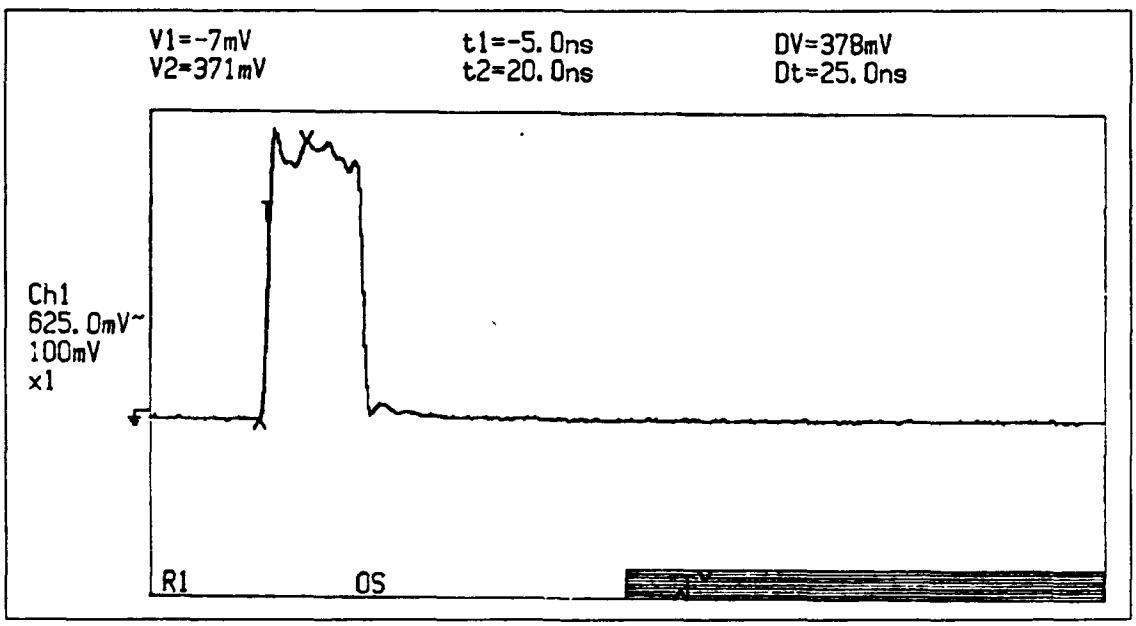

Figure 5. Waveform of source A - laser source.

For the remainder of this thesis, the waveforms in Figure 5 and Figure 6 will be referred to as source A and B, respectively.

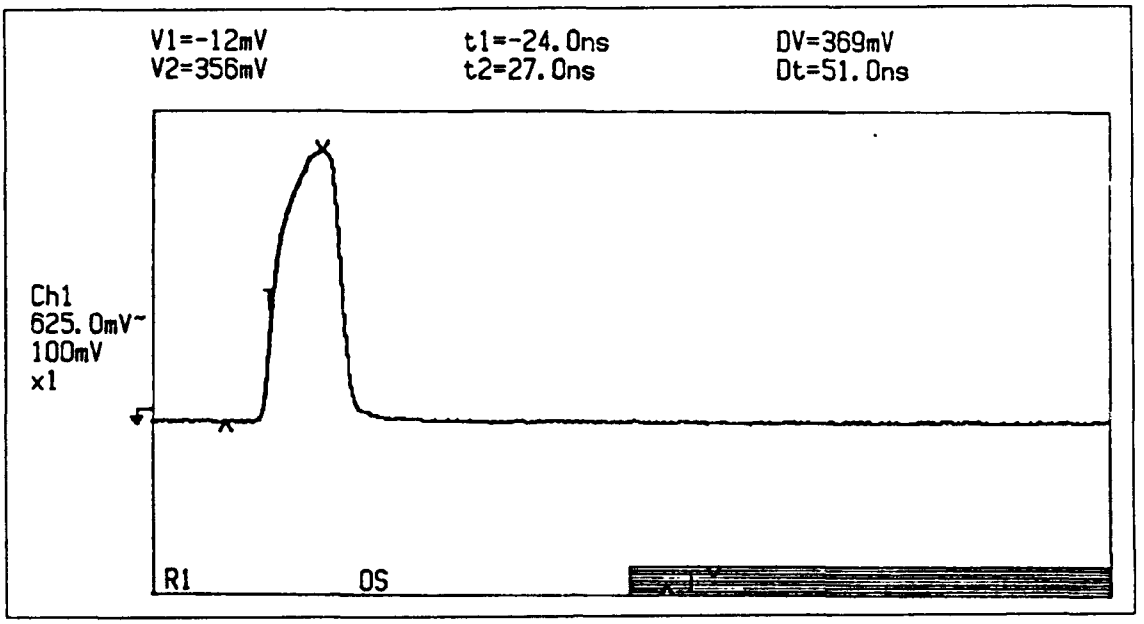

Figure 6. Waveform of source B - LED source.

Not apparent in the figures is the attenuation added to the laser light in order to obtain equal amplitudes of these two source signals. Because waveform A was produced using a laser diode, it was attenuated to a level equal to that of the LED source so that the cross-correlation properties of the two sequences could be observed. Using Appendix A, which will be discussed in a following section, we have determined that waveforms A (attenuated) and B contain optical power levels of –4.2 dBm and –4.5 dBm, respectively.

3. Fiber

We have a choice between single-mode and multimode fiber, either of which could be a step or graded index. This choice depends on the type of light source used and on the amount of dispersion that can be tolerated. LEDs tend to be used with multimode fibers, although some specialized LEDs (edge-emitting) can launch sufficient power into a single-mode fiber. The amount of optical power that can be coupled into an optical fiber from an LED depends on the core-cladding index difference, which is related to the numerical aperture of the fiber. As the numerical aperture of the fiber increases, the amount of power coupled into the fiber also increases [Ref. 14: p. 318].

Either a single-mode or a multimode fiber can be used with a laser diode. A single-mode fiber can provide extremely high bit rate-distance-products. However, a disadvantage of single-mode fibers is that the small core size, typically 5 to 16 μm in diameter, makes splicing and power coupling more difficult than for multi-mode fibers having diameters of 50 μm and greater. [Ref. 14: p. 319].

The decision to utilize 50 μm multimode fiber for this thesis was based on two factors. First, because of the difficulties associated with splicing single-mode fiber, and considering the large number of connectors used in the data link, multimode fiber is preferred. Second, it was already available in large quantities in the laboratory.

4. Detector

In choosing a particular photodetector, we mainly need to determine the minimum amount of optical power that must fall on the device to allow signal detection.

This is usually specified by the device's sensitivity rating, given in dBm. Again, there are two types of photodetectors available, the *pin* photodiode and the avalanche photodiode (APD). The *pin* photodiode receiver is simpler, more stable with changes in temperature, and less expensive than an APD receiver [Ref. 14: p. 318]. However, the advantages of a *pin* photodiode receiver may be overruled by the increased sensitivity of the APD if very low optical power levels are to be detected [Ref. 14: p. 318].

A variety of manufacturers offer optical receivers ready for use in the laboratory. Much of this equipment incorporates variable range settings with calibrated outputs. For this thesis, a Photodyne model 1600XP waveform analyzer was utilized as the receiver. A high speed Germanium APD is the basic detector and is followed by a wideband transimpedance amplifier. This particular piece equipment offers three range settings. Table 2 indicates the output and input parameters for the various ranges.

TABLE 2. WAVEFORM ANALYZER RANGE SETTINGS (From Ref. 16: p. 8).

INPUT POWER	RANGE SETTING	OUTPUT VOLTAGE
0.1 μW to 10μW	100 mV / μW	10 mV to 1 V
1 μW to 100μW	10 mV / μW	10 mV to 1 V
10 μW to 1 mW	1 mV / μW	10 mV to 1 V

From Table 2 we can see that the input optical power is given in microwatts for a given output voltage level. Referencing this input power to 1 mW, we can easily relate the output receiver voltage to input optical power in dBm. Appendix A provides a

tabulated form of this relationship for the three given ranges. This table provides a quick reference for finding the input optical power for a given receiver output voltage level.

5. Power Budget

We start the power budget analysis with the model for the data link shown in Figure 4. The model considered losses due to all parameter mismatch, such as incompatible fiber-core diameters, numerical apertures, Fresnel losses, and coupling misalignments. Varying fiber attenuations due to the different delay-line lengths and splitting losses were also considered. This particular approach was used initially but obtaining accurate results became tedious. Theoretical values varied compared to actual values obtained in the laboratory. The effects of the non-uniform splitting-losses combined with the different delay line lengths also made this approach unnecessarily complicated.

An alternative approach, which first uses an ideal model and treats signals as sequences instead of pulses, provided a simpler overview of the power budget problem. Once the conceptual model was realized, it was updated with actual component loss values providing more accurate results. This method is presented here in an effort to provide a clearer understanding of the losses incurred within the data link.

In Chapter two we stated that sequences can be represented using vector notation. For this thesis all sequences have a weight of four. Therefore all sequence vectors will contain four non-zero values. A similar notation can be used to represent the optical power of each pulse in the sequence. Taking this concept a step further, losses

incurred on the pulses within a sequence can also be represented using this notation. We proceed with the power budget model using this notation.

The initial pulse launched into the first 1×4 splitter is divided into four pulses. The splitting losses (in dB) incurred on each of these four pulses is represented in vector form as $l = [-6 \ -6 \ -6 \ -6]$. At this point, considering an ideal model, we assume a uniform distribution of attenuation and coupling loss across the 4 delay lines of −2 dB. The cumulative losses are now $l = [-8 \ -8 \ -8 \ -8]$. The second splitter contributes another −6 dB to the loss sequence giving a total loss experienced by an encoder as $l = [-14 \ -14 \ -14 \ -14]$. The 2×2 splitter contributes −3 dB to the loss vector giving $l = [-16 \ -16 \ -16 \ -16]$. This vector represents the total amount of attenuation experienced by the code sequence before it arrives to the input of a decoder.

As each sequence enters a decoder, it experiences losses similar to those seen in the encoder. The first splitter contributes another −6 dB; however, because we now have four sequences, it is easier to represent l in matrix form

$$l = \begin{bmatrix} -22 & -22 & -22 & -22 \\ -22 & -22 & -22 & -22 \\ -22 & -22 & -22 & -22 \\ -22 & -22 & -22 & -22 \end{bmatrix} \tag{9}$$

where each row in the matrix represents one of the four sequences produced by the decoder's first 1×4 splitter. The 4 delay lines, for this ideal model, contribute another −2 dB of attenuation. Finally the last splitter contributes another −6 dB giving

$$I = \begin{bmatrix} -30 & -30 & -30 & -30 \\ -30 & -30 & -30 & -30 \\ -30 & -30 & -30 & -30 \\ -30 & -30 & -30 & -30 \end{bmatrix} . \qquad (10)$$

These losses may seem extreme; however we must now take the correlation effect into account. We stated earlier that the delay lines are selected such that one of the four pulses of each of the four sequences are coincident on the output lead of the splitter. Specifically, the first pulse of the sequence that experiences the longest delayed arrives at the output of the decoder at the same instant as the last pulse of the sequence experiencing the shortest delay. Intermediate pulses of the intermediate sequences are delayed accordingly. If the first and last rows of matrix *I* represent the fastest and slowest sequences, respectively, then the coincident pulses are on the left diagonal of matrix *I*. The addition of the optical power contained in these four pulses produces a pulse with an power level four times greater (+6 dB) than the individual pulses. This represents the spike, or main lobe, of the autocorrelation waveform. Also, because of the orthogonal properties of the code sequences, no other pulses are coincident. Consequently, pulses above and below the left diagonal fall out to the right and left of the main lobe, respectively. The losses incurred on the final correlated sequence are represented as follows

$$I = [-30, -30, -30, -30, -30, -30, -24, -30, -30, -30, -30, -30, -30] . \qquad (11)$$

This sequence shows that a spike four times the amplitude of the side lobe pulses is present. However, it does not indicate the relative spacing between the pulses. In Chapter 4 and 5 the relative spacing between the pulses is addressed with the design and implementation of the encoders and decoders.

IV. ENCODERS

A. DESIGN

The starting point for the design of the encoders is to examine the code sequences that must be generated. From a graphical representation, it can be easily seen where the pulse placement is within the sequences. Since the placement of the pulses are multiples of the chip time, we need only to determine the length of fiber needed to impose a delay of one chip interval. It then follows that to generate successive delay intervals, we need only take multiples of this length. Table 3 shows the two desired sequences and the required delay needed for proper pulse placement.

TABLE 3. GRAPHICAL REPRESENTATION OF CODE SEQUENCES.

g(2,4)														
X	1	0	0	1	0	0	0	0	0	0	0	0	1	1
delay units	0			3		5		7				11	12	13
Y	1	0	0	0	0	1	0	1	0	0	0	1	0	0

To determine the length of fiber required to impose a delay of 50 ns, we start by establishing the speed of light in an optical fiber, v, with an index of refraction, n, of 1.47.

$$v = \frac{c}{n} = \frac{3\times10^8}{1.47} = 2.04\times10^8 \text{ m/s.} \tag{12}$$

Taking the speed of light in the fiber and multiplying it by one delay unit of time, 50 ns, we calculate the length of fiber required to impose a delay of one chip interval.

$$d = s \cdot t = \left(2.04 \times 10^{8}\right)\left(50 \times 10^{-9}\right) = 10.197 \text{ m.} \tag{13}$$

Multiples of this length can then be put into tabular form for quick reference. Table 4 provides these results.

TABLE 4. DELAY LINE LENGTHS.

Chip time = 50.00E–9	
Delay required	Length in meters
0	0
1	10.197
2	20.394
3	30.591
4	40.788
5	50.985
6	61.182
7	71.379
8	81.576
9	91.773
10	101.97
11	112.17
12	122.36
13	132.56

For the two sequences $\underline{X}$ and $\underline{Y}$ displayed in Table 3 with a chip time equal to 50 ns, we summarize the calculated encoder delay line lengths in Table 5. Note that a delay line equal to zero in simply the direct connection of two splitters.

TABLE 5. ENCODER DELAY LINE LENGTHS.

g(2,4)	Sequence $\underline{X}$	Sequence $\underline{Y}$
Pulse no.	Length in meters	Length in meters
1	0.0	0.0
2	30.591	50.985
3	122.36	71.379
4	132.56	112.17

B. IMPLEMENTATION

Up to this point, all conditions placed on the data link design have been considered ideal. For example, the code sequences considered have had uniform pulse amplitudes. Uniform splitting losses across the 1×4 splitters have also been assumed. Also, the delay lines have been assumed to impose uniform losses. However, the reality of the design is far from ideal.

For example, the 1×4 splitters do not have a uniform -6 dB loss from the input to output lead. Non-uniform splitting losses combined with excess losses within the devices produce nonideal losses from input to each output. The varying lengths of the delay lines also impose different attenuation on each respective pulse. Also, mechanical connectors can insert losses as high as -3 dB if not carefully assembled.

The direct assembly of two 1×4 splitters and the three delay lines produced a sequence of varying amplitude. While this effect is not strictly adverse, it makes the design of the decoder much more difficult. Sequences with uniform amplitude pulses are preferred.

To deal with the problem of nonuniform losses associated with the encoder components, assembly was accomplished using an insertion loss approach. Once the delay lines were cut and connectors joined to the fiber ends, we inserted the length of fiber between a source with a known power level and an optical power meter. A measurement of the actual insertion loss could then be taken. For excessive insertion loss, say greater that -2 dB, the fiber connectors were repolished or replaced until acceptable levels are achieved. The attenuation specification from the fiber manufacturer, given in dB/km, was used to arrive at some preliminary loss level and losses of greater value were considered as a result of the connectors. For this thesis, fiber with an attenuation of -2.8 dB/km was used. This indicates that the longest delay line (132.5 m), ideally, would impose an attenuation level of -0.371 dB. However, for SMA-style connectors, this level of attenuation is unrealistic and unattainable. Losses in the vicinity of -1 dB per delay line are more realistic and acceptable.

This same technique was also used with each of the 1×4 splitters. Each splitter was connected to a source of known power level and the loss across each of the output leads was recorded. Appendix B contains the measured results for all eight 1×4 splitters used.

With the insertion losses tabulated for all components used in the link, optimum assembly can proceed. For the first encoder, the problem of component selection can be stated as follows. From the eight splitters available, which two, combined with the three designated delay lines (the fourth being zero), and which corresponding leads will give a uniform distribution of losses, producing a pulse sequence with near equal amplitudes. The number of different combinations is large; however, not unsolvable.

Using a computer program, such as MATLAB, an optimum combination can be determined. Appendix C lists the MATLAB source code and initial data file that was used. A matrix containing the measured losses of the splitters (in row vector format) was loaded into the MATLAB environment. The measured losses for the delay lines are represented with vector *b*. The program assigns two unequal row vectors to variables *r1* and *r2*. The three vectors (*b, r1*, and *r2*) are added and the standard deviation was taken of the sum. If the standard deviation was less than the previous stored value, the three vectors were stored for output. The vectors were rotated right four times (similar to a circular buffer operation), one at a time, and a new sum was computed. The standard deviation was taken and compared. The process continues for all vectors in the matrix.

Once an optimum combination was determined for a given set of delay lines (vector *b*), the data file, loop indexes *l* and *m*, and the delay line vector *b* were updated. This process was carried out four times, once for each encoder and decoder. Results for the two encoders are summarized in Table 6 below.

TABLE 6. ENCODER'S ORDER OF ASSEMBLY.

Encoder X	Measured losses (in dB)$_{\text{output lead number}}$			
ID # 580	-7.0_1	-6.5_4	-7.3_2	-7.1_3
ID # 586	-7.7_4	-7.7_1	-6.9_3	-6.8_2
Delay line losses	0.0_1	-0.5_2	-0.7_3	-0.9_4
Sum of losses	-14.7	-14.7	-14.9	-14.8
Encoder Y	**Measured losses (in dB)$_{\text{output lead number}}$**			
ID # 582	-7.4_1	-7.1_4	-6.4_2	-6.1_3
ID # 584	-6.8_1	-6.2_3	-7.2_2	-7.1_4
Delay line losses	-0.0_1	-0.9_2	-1.2_3	-1.5_4
Sum of losses	-14.2	-14.2	-14.8	-14.7

Appendix B lists the measured losses from input lead to each output lead for each of the 1 ×4 splitters. In Table 6, the subscripts are used to indicate which output lead of the splitter the corresponding loss refers to. For the delay lines, a subscript of 1 corresponds to the shortest of the encoder delay lines set while a subscript of 4 corresponds to the longest.

C. PERFORMANCE

Output waveforms for the two encoders are shown in figures 7 and 8 respectively. Two important questions are worth asking when reviewing these waveforms. First, are all the pulses located where they should be? Second, are the amplitudes of the pulses acceptably equal?

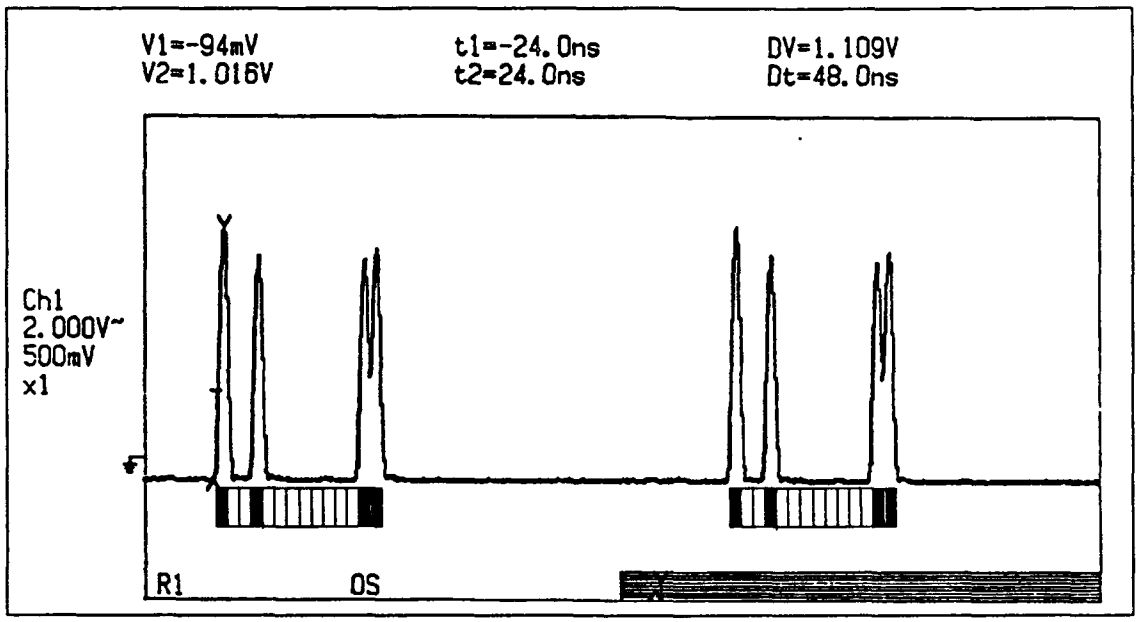

Figure 7. Sequence X.

To determine if the pulses are spaced according to the codes specified, a band diagram has been inserted below each waveform to give a clearer perspective as to the pulse spacing. The dark areas correspond to the desired positions of the pulses within the sequence. It can clearly be seen that all pulses are located at the correct positions forming the desired code sequences X and Y.

To determine if the sequence pulses are nearly equal, we start by observing the receiver voltage level of the first pulse in the sequence. Typically, the first pulse in the sequence experiences the least amount of loss. From Figure 7 we see that the first pulse in sequence X has a receiver voltage level of 1.103 volts. Using Appendix A, we can extrapolate a power level from the 100 mV/uW range column of approximately −19.5 dBm. From Table 6 we can see that the first pulse in sequence X should experience a

−14.7 dB loss from the source level. From Figure 5 an initial power level of −4.2 dBm was measured. Thus, the power level of the first pulse in sequence X should be −18.7 dBm. The difference between the expected value and the measures value is only −0.6 dBm. The remaining pulses in the sequence do experience slightly more attenuation that expected. This is attributed to higher than expected coupling losses between the splitters and the delay lines.

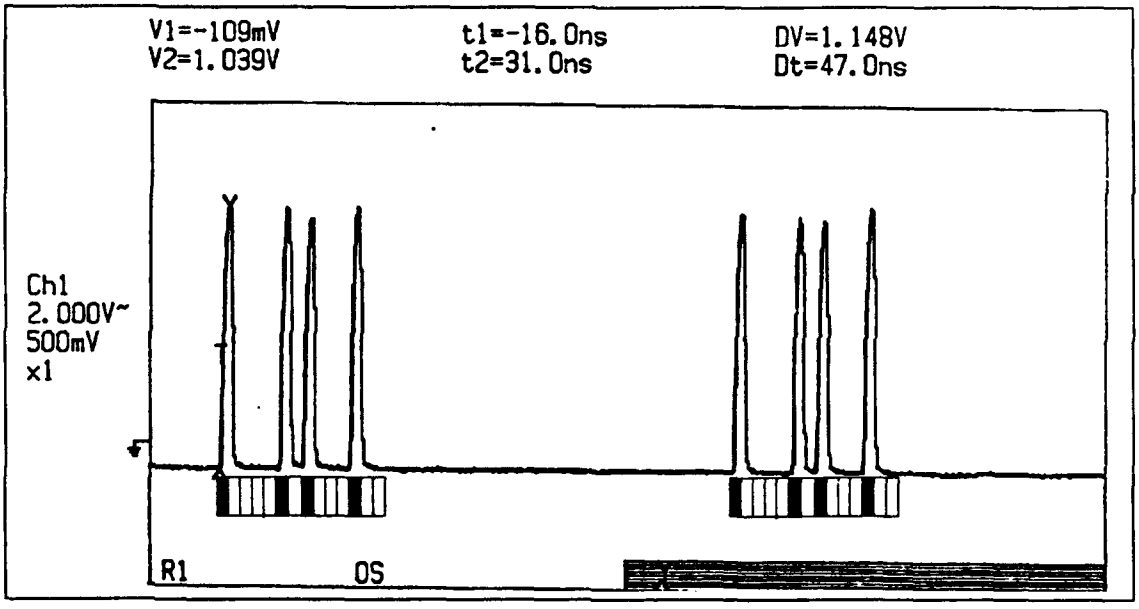

Figure 8. Sequence Y.

From Figure 8 we see that the first pulse in sequence Y has a receiver voltage level of 1.148 volts. Again using Appendix A, we can extrapolate a power level from the 100 mV/uW range column of approximately −19.3 dBm. From Table 6 we can see that the first pulse in sequence Y should experience a −14.2 dB loss. From Figure 6 an

initial power level of −4.5 dBm was measured. Here the resultant power level should be −18.7 dBm. Again the difference is only −0.6 dBm. The amplitudes of the remaining pulses in the sequence are within 30 mV indicating more losses.

In this Chapter we demonstrated that the generation of optical sequence using delay lines is possible. The precise placement of pulses within the sequence was not a major problem. However, unequal splitting and delay line losses make assembly of the encoders similar to a jigsaw puzzle. The techniques used to implement the encoders will be briefly discussed again in Chapter 5 which describes the implementation of the decoders.

V. DECODERS

A. DESIGN

Reference 17 discusses optimal detection of discrete signals in great detail. These principles can also be applied here. Thus, detection can be accomplished using a matched filter. The matched filter can be viewed as a reversed, conjugate replica of the signal [Ref. 17: p. 372]. The sequences that must be detected are displayed in Table 3. Taking the mirror image of the sequences gives a graphical representation of the matched filters needed for detection. The sequences displayed in Table 7 represent the impulse response of the two matched filters.

TABLE 7. GRAPHICAL REPRESENTATION OF MATCHED FILTERS.

$\underline{X}^{-1}$	1	1	0	0	0	0	0	0	0	0	1	0	0	1
delay units	0	1			4		6				10	11		13
$\underline{Y}^{-1}$	1	0	0	0	1	0	1	0	0	0	0	1	0	0

To determine the length of the delay lines for each decoder, we first observe the number of delay units associated with each of the pulses in the sequences. Using Table 7, this is easily determined. The number of delay units is then used as table entries into Table 4 to obtain the required lengths. The decoder delay-line lengths are summarized in Table 8. Again, note that delay lines equal to zero are simply a direct connection between the two splitters.

TABLE 8. DECODER DELAY LINE LENGTHS.

g(2,4)	Sequence $\underline{X}^{-1}$	Sequence $\underline{Y}^{-1}$
Pulse no.	Length in meters	Length in meters
1	0.0	0.0
2	10.197	40.788
3	101.97	61.182
4	132.56	112.17

B. IMPLEMENTATION

In implementing the decoders, we follow the same procedures and precautions used for the encoders. The MATLAB program used to sort through component combinations for the encoders is also used to find the optimum component combinations for the decoders. Results for the two decoders are summarized in Table 9.

These results represent an effort to minimize component mismatch, thus reducing large variations in sequence amplitudes. However, the actual assembly of the components selected may, initially, produce somewhat less than optimum results. Patience and attention to detail when working with mechanical connectors must be adhered to in obtaining optimum (or near optimum) results. With this in mind, waveform variations are expected and should not be scrutinized too severely. Amplitude variations within 5 or 10% are considered acceptable.

TABLE 9. DECODER'S ORDER OF ASSEMBLY.

Decoder X^{-1}	Measured losses (in dB)$_{\text{output ead number}}$			
ID # 585	-7.5_4	-6.9_3	-6.9_2	-7.6_1
ID # 587	-7.7_4	-7.2_2	-6.9_3	-6.3_1
Delay line losses	-0.0_1	-1.5_2	-1.6_3	-1.5_4
Sum of losses	−15.2	−15.6	−15.4	−15.4
Decoder Y^{-1}	Measured losses (in dB)$_{\text{output ead number}}$			
ID # 581	-7.4_4	-7.4_1	-6.8_2	-6.3_3
ID # 583	-7.5_2	-6.7_3	-6.3_1	-7.5_4
Delay line losses	-0.0_1	-1.0_2	-1.6_3	-1.8_4
Sum of losses	−14.9	−15.1	−14.7	−15.6

C. PERFORMANCE

In this section we examine the performance of the decoders in a manner similar to that used for the encoders. We first must establish that the correct delays have been implemented and that the losses are within acceptable limits. Verification of these parameters ensures that the correlation of any input sequences will be predictable. In Chapter 6 the decoder's correlation properties will be examined more thorough.

To establish that the correct delays are being imposed by the decoders, we simply injected a single pulse (50 ns) to each of the decoders inputs. This has an effect of producing a sequence that represents the impulse response of the two filters. The expected outputs are the inverse sequences displayed in Table 7. Output waveforms for the two decoders are displayed in Figures 9 and 10.

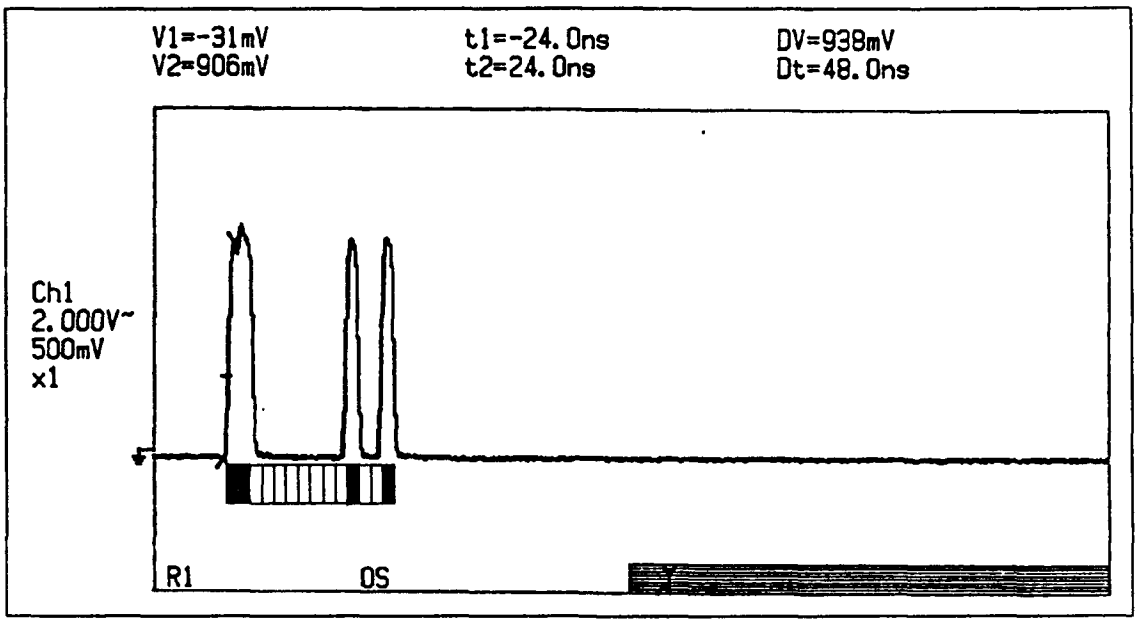

Figure 9. Impulse response for decoder - sequence X^{-1}.

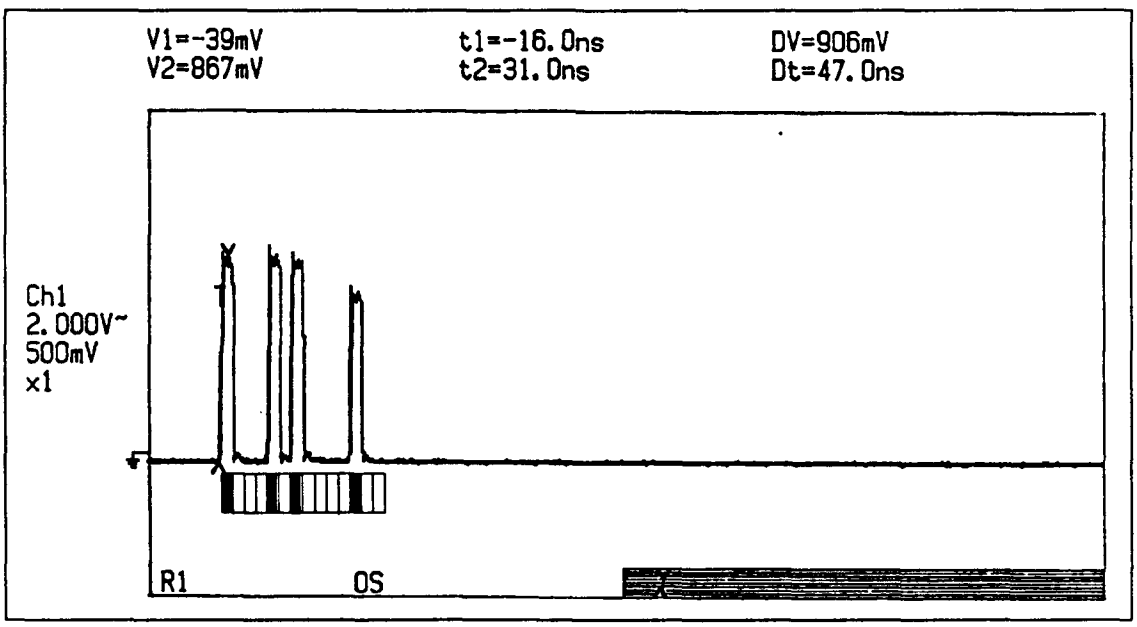

Figure 10. Impulse response for decoder - sequence Y^{-1}.

Because a grid has not been provided with the waveforms, a band diagram has been inserted below each waveform to aid in examining pulse placement. It is apparent that all pulses are located in their correct positions.

To determine if the decoders are adding an excess attenuation, we follow the same steps used in the examination of the encoders. From Figure 9 we see that the first pulse in the sequence has a receiver voltage level of 938 mV corresponding to an optical power level of approximately −20.3 dBm. From Table 9 we can see that the first pulse in sequence $\underline{X}^{-1}$ should experience a −15.2 dB loss from the source level. With an initial measured power level of −4.2 dBm, the power level of the first pulse should be −19.4 dBm. Here the difference is only −0.9 dBm. The remaining pulses in the sequence are within 40 mV to this power level and are considered acceptable.

From Figure 10 we see that the first pulse in the sequence has a voltage level of 906 mV corresponding to an optical power level of approximately −20.3 dBm. From Table 9 we can see that the first pulse in sequence $\underline{Y}^{-1}$ should experience a −14.9 dB loss. With an initial power level of −4.2 dBm, the resultant power level should be −19.1 dBm. For this decoder, the difference is −1.2 dB. Here the ill effects of mechanical couplers can clearly be seen. Incurred losses within the entire sequence, and more so for the last pulse, are slightly higher than results for any of the other assemblies.

The successful implementation of the decoders was completed using techniques discussed in the Chapter 4. Again the major obstacle was dealing with unequal splitting

and delay line losses. In Chapter 6 a more detailed discussion of the decoder's correlation properties and the system's overall performance will be addressed.

VI. RESULTS

A. AUTOCORRELATION

With the encoders and decoders assembled and functioning properly, the next step was to complete the data link by joining the individual assemblies. Thus far, our efforts have been to produce waveforms that have been described by Equations 6 and 7. However, while these equations represent the sequence properties, they do not define exactly how each of the decoder's output waveforms should appear. With careful attention to the delays, we generated a graphical representation of the autocorrelation and cross-correlation of the sequences in question and verified correct operation of the data link.

Figure 11 shows the number of delays introduced by the encoder and decoder for sequence $\underline{X}$. For the encoder, there is a direct correspondence between the numeric delay values and the pulse locations within the sequence shown in row one of Table 10. For the decoder, the numeric delays represent delayed shifts of the entire sequence. The shifted versions of sequence $\underline{X}$ can be seen in rows three through six in Table 10. The combining effect of the decoder can be seen in the last row of Table 10. This sequence represents the autocorrelation of sequence $\underline{X}$ and is the desired output waveform. Figure 12 shows the actual output waveform and it can clearly be seen that the last row in Table 10 and this waveform are similar.

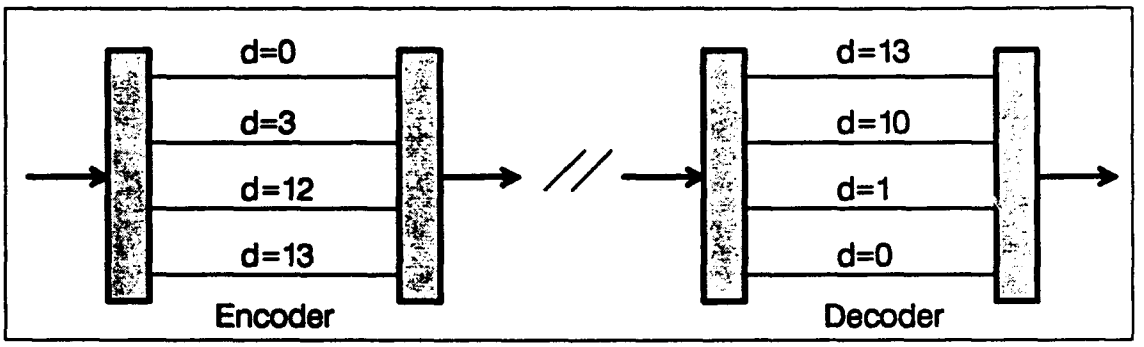

Figure 11. Encoder and decoder delays for sequence X.

TABLE 10. AUTOCORRELATION OF SEQUENCE X.

1	0	0	1	0	0	0	0	0	0	0	0	1	1																	
1	0	0	1	0	0	0	0	0	0	0	0	1	1																	
	1	0	0	1	0	0	0	0	0	0	0	1	1																	
										1	0	0	1	0	0	0	0	0	0	0	0	1	1							
													1	0	0	1	0	0	0	0	0	0	0	0	1	1				
1	1	0	1	1	0	0	0	0	0	1	0	1	4	1	0	1	0	0	0	0	0	1	1	0	1	1				

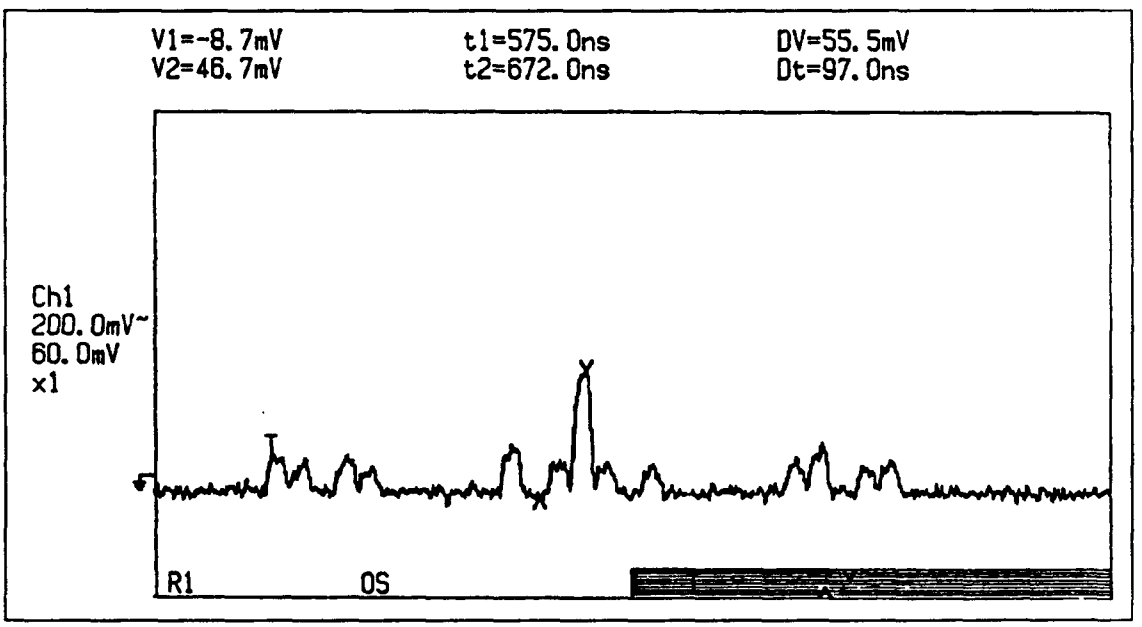

Figure 12. Autocorrelation waveform for sequence X.

In Figure 12 we can also see that the amplitude of the main lobe is 55.5 mV. Using Appendix A to convert this voltage level to optical power gives −31.2 dBm. This power level represents a −27.01 dB attenuation of the original source pulse. Side lobes have been verified to be approximately −37.0 dBm; down −6 dB from the main lobe. These levels are somewhat better than initial expectations.

For sequence Y we follow the same steps as above. Figure 13 shows the delays used in the encoder and decoder for sequence Y. Table 11 displays the relationship between the encoder delays and the sequence pulses, and the decoder and the shifted versions of the sequence. Again, the last row of Table 11 represents the autocorrelation of sequence Y. This waveform is directly compared with the waveform shown in Figure 14 which shows the correct output.

B. CROSS-CORRELATION

A graphical representation of the cross-correlation waveforms can be created by applying each of the decoder's delays to the opposite sequence. Figure 15 and Table 12 show decoder delays for sequence Y being applied to sequence X. Again, the last row of Table 12 represents the resultant waveform that is similar to the waveform displayed in Figure 16.

For the second waveform, decoder delays for sequence X are applied to sequence Y. Figure 17 and Table 13 show these results. The last row of Table 13 represents the resultant waveform, which is similar to the waveform displayed in Figure 18.

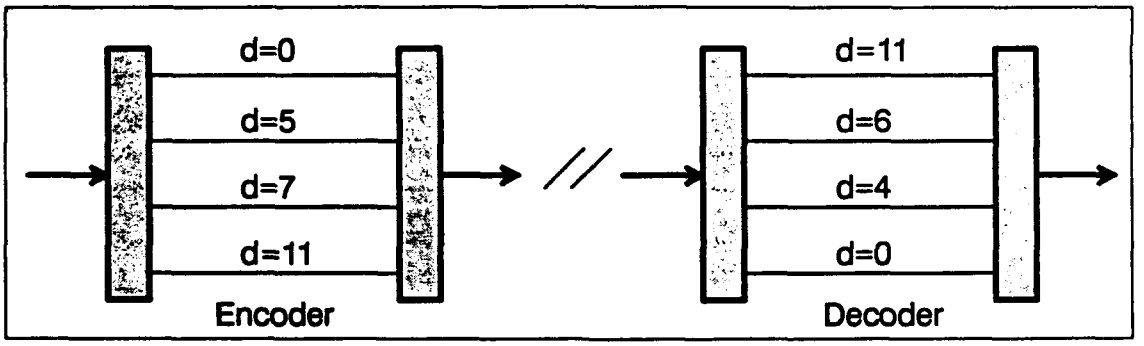

Figure 13. Encoder and decoder delays for sequence Y.

TABLE 11. AUTOCORRELATION OF SEQUENCE Y.

1	0	0	0	0	1	0	1	0	0	0	1	0	0	
1	0	0	0	0	1	0	1	0	0	0	1	0	0	
	1	0	0	0	0	1	0	1	0	0	0	1	0	0
		1	0	0	0	0	1	0	1	0	0	0	1	0	0
			1	0	0	0	0	1	0	1	0	0	0	1	0	0
1	0	0	0	1	1	1	1	0	1	0	4	0	1	0	1	1	1	1	0	0	0	1	0	0

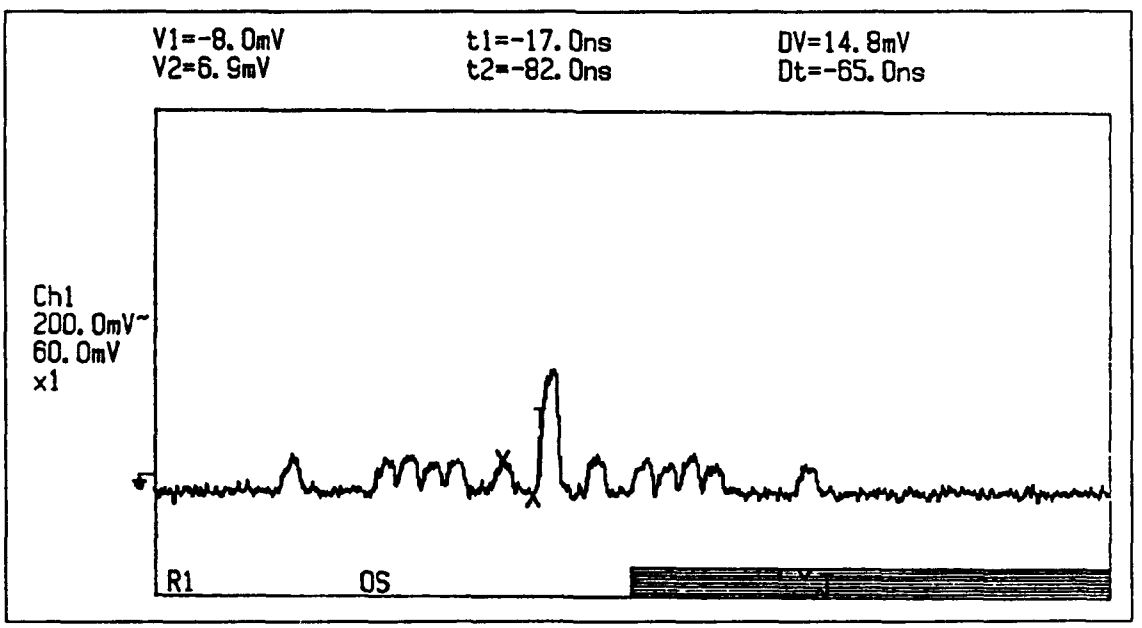

Figure 14. Autocorrelation waveform for sequence Y.

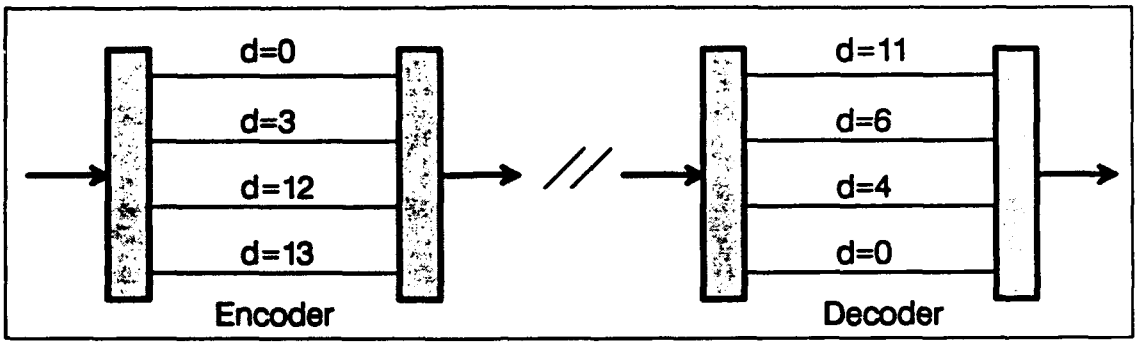

Figure 15. Encoder delays for sequence X and decoder delays for sequence Y.

TABLE 12. CROSS-CORRELATION OF SEQUENCE X AND Y.

1	0	0	1	0	0	0	0	0	0	0	0	1	1	
1	0	0	1	0	0	0	0	0	0	0	0	1	1	
			1	0	0	1	0	0	0	0	0	0	1	1
					1	0	0	1	0	0	0	0	0	0
							1	0	0	1	0	0	0	0
1	0	0	1	1	0	1	1	0	1	0	1	1	1	1

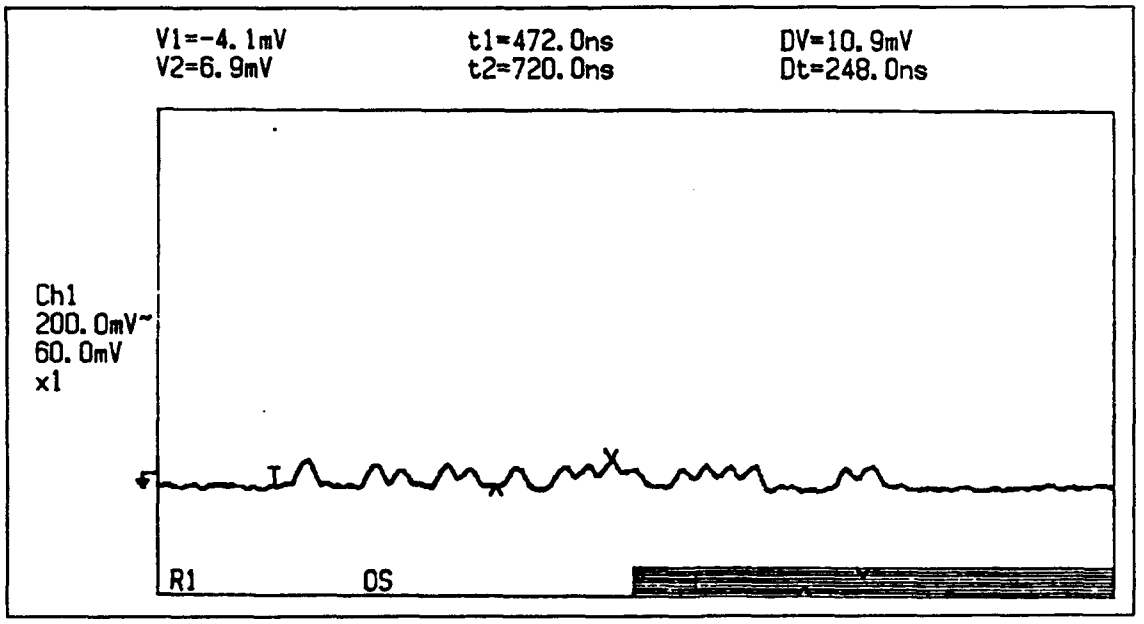

Figure 16. Cross-correlation waveform for sequence X and decoder Y.

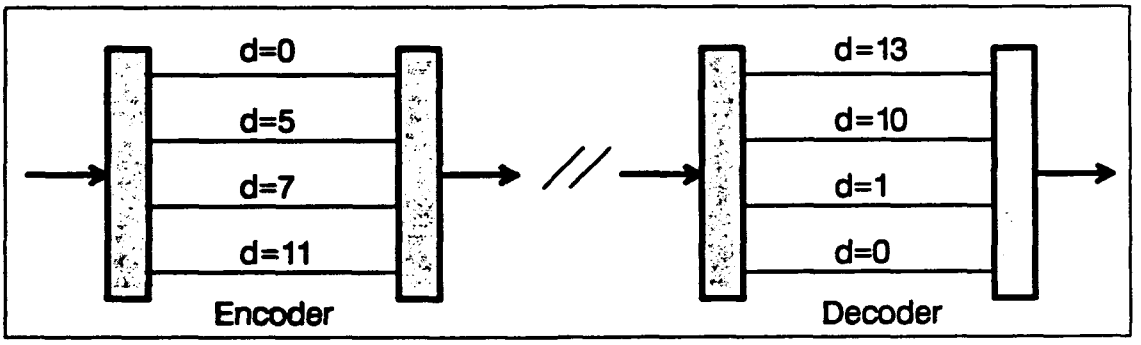

Figure 17. Encoder delays for sequence Y and decoder delays for sequence X.

TABLE 13. CROSS-CORRELATION OF SEQUENCE Y AND X.

1	0	0	0	0	1	0	1	0	0	0	1	0	0	
1	0	0	0	0	1	0	1	0	0	0	1	0	0	
	1	0	0	0	0	1	0	1	0	0	0	1	0	0
						1	0	0	0	0	1	0	1	0	0	0	1	0	0	
									1	0	0	0	0	1	0	1	0	0	0	1	0	0
1	1	0	0	0	1	1	1	1	0	1	1	1	1	0	1	0	1	1	0	1	1	0	0	1	0	0

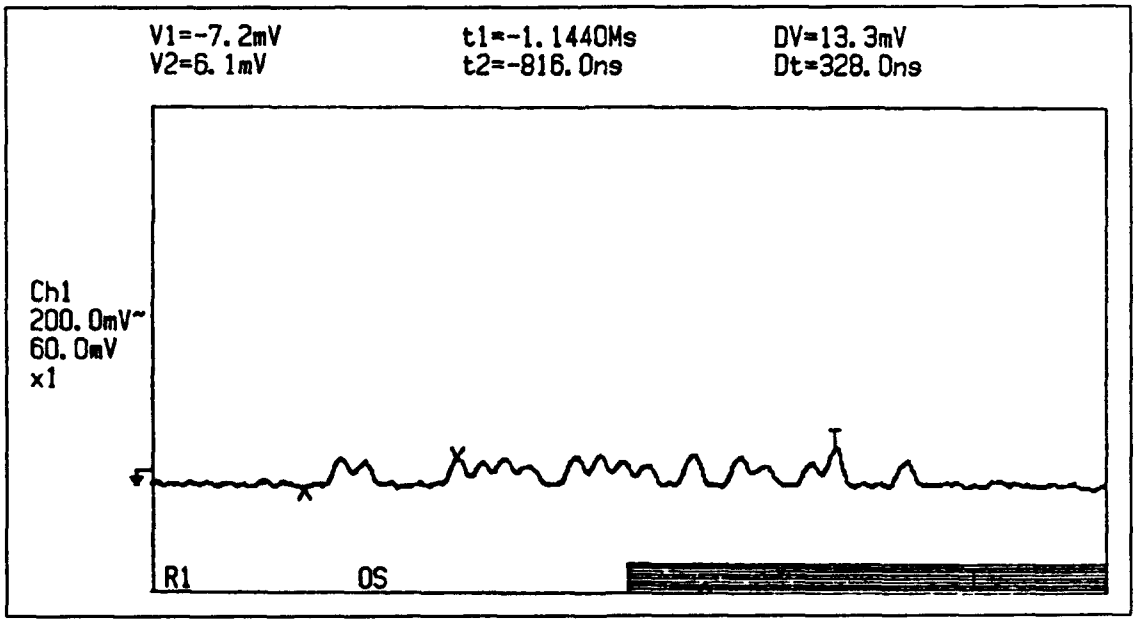

Figure 18. Cross-correlation waveform for sequence Y and decoder X.

Figures 19 and 20 display simultaneous operation of the sources. From these waveforms the asynchronous transmission of data bits can be seen. However, there is an increase in the coincidence of pulses between the two correlated waveforms. This effect raises the probability of error. As long as the weight of the sequences is less than the number of users, the probability for error is held to a minimum. For further information on probability of error, References [5], [6], and [12] provide some quantitative arguments on the probability density functions associated with asynchronous interfering OOCs.

C. CONCLUSIONS

This research represents the first iteration in the design and implementation of a fiber optic data link employing a code division multiple access scheme using fiber optic delay lines. The initial objectives of this thesis have been met and are summarized below with several additional observations.

A general understanding of orthogonal optical codes and their properties was achieved. The application of these codes and, specifically, the generation of optical sequence using delay lines were successfully demonstrated. The precise placement of pulses within the sequence was not a major problem. Exact delay line lengths were not critical because of the relatively wide pulse width (50 ns) that was used. The major obstacle, related to encoder and decoder realization, were the unequal splitting losses of the 1×4 splitters and the attenuation associated with the different delay line lengths. Also, the SMA-style mechanical couplers that were used in this thesis proved to be

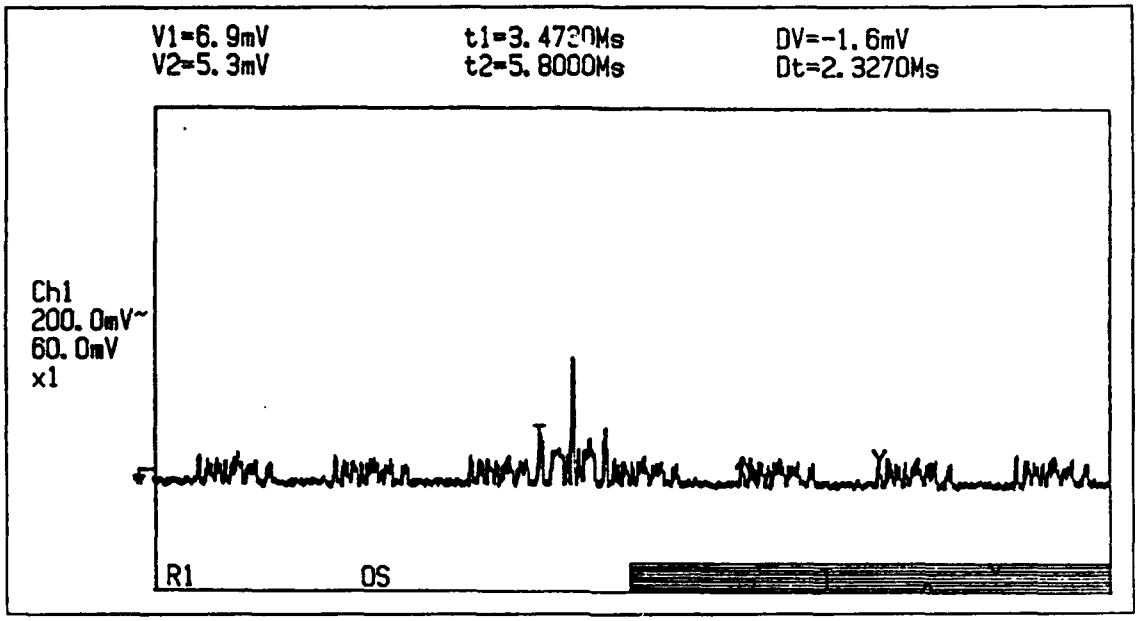

Figure 19. Simultaneous operation.

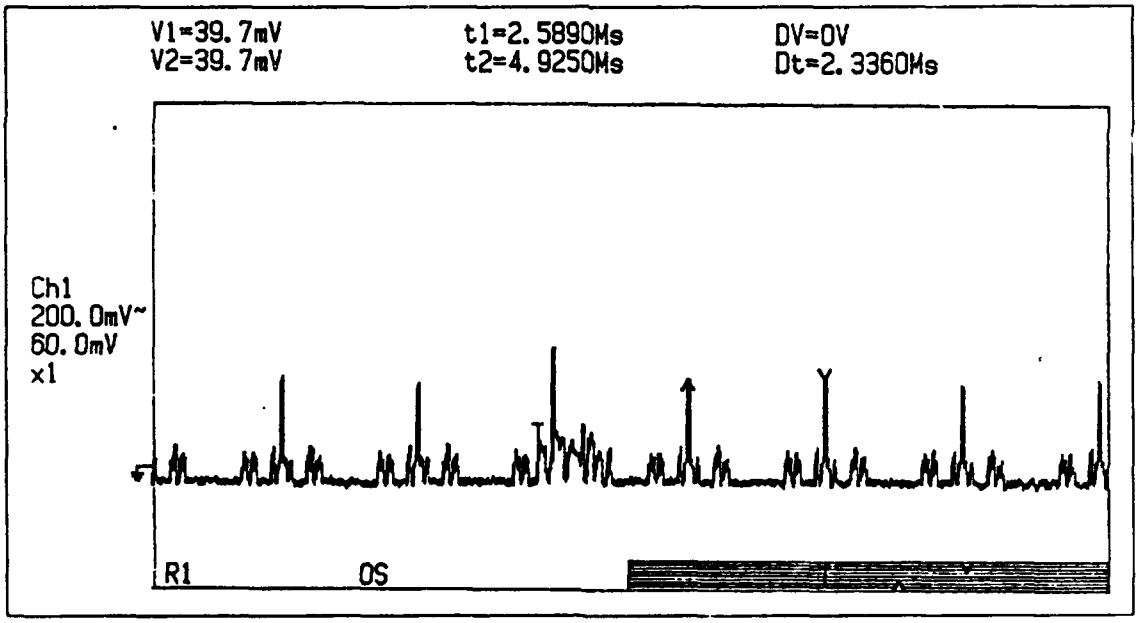

Figure 20. Simultaneous operation.

temperamental causing system and subsystem performance to vary substantially.

The decoding process demonstrated the orthogonal properties of the codes that were used. Waveforms were verified to be correct with the use of graphical diagrams. The high losses inherent with this particular scheme were also observed in the final waveforms. Overall system performance showed that FO-CDMA can provide asynchronous, multiple access communication that can be implemented in local area networks. An advantage of the delay line approach used in this thesis was the lack of network control between transmitter and receiver, thus reducing complexity and eliminating the speed limitations of conventional CDMA schemes.

Another observation of the FO-CDMA data link is the unique security advantage provided by the coding and the inherent properties of optical fiber. However, these advantages alone are not without expense. The main detriment with the parallel delay line method for encoding and decoding is the high losses due to the numerous splitters and connectors used in the encoders and decoders. This tends to render low-cost, low-power, sources and receivers useless for such applications.

A final observation worthy of discussion is the maximum data rate achievable with this particular implementation. An important fact when viewing the correlated waveforms is the time duration from the start of the first chip to the end of the last chip. From the graphical representations of the correlated waveforms, we see that the total time for correlation is $(L+(L-1))$. Thus, this reduces the assumed data rate to roughly one half. For this implementation a data rate of 740 kb/s is achievable without correlation

overlap. Also, because sequence lengths vary within a set, it appears that it is also code dependent. As such, shorter sequences within a set can transmit data at higher rates.

The gap between maximum and reasonable performance is wide. To take full advantage of the capabilities this scheme offers requires a commitment to hardware resources. With higher-power, faster, and more efficient components, more users can be supported at higher data rates. Additionally, overcoming some of the implementation drawbacks with alternate approaches of encoding and coupling would greatly improve the feasibility of practical applications.

APPENDIX

A. VOLTAGE TO OPTICAL POWER CONVERSION TABLE

Page 1	Range		
	100mV / uW	10mV / uW	1mV / uW
Output Voltage	DBM	DBM	DBM
0.010	-40.00	-30.00	-20.00
0.027	-35.72	-25.72	-15.72
0.044	-33.61	-23.61	-13.61
0.060	-32.19	-22.19	-12.19
0.077	-31.13	-21.13	-11.13
0.094	-30.27	-20.27	-10.27
0.111	-29.56	-19.56	-9.56
0.127	-28.95	-18.95	-8.95
0.144	-28.41	-18.41	-8.41
0.161	-27.93	-17.93	-7.93
0.178	-27.50	-17.50	-7.50
0.195	-27.11	-17.11	-7.11
0.211	-26.75	-16.75	-6.75
0.228	-26.42	-16.42	-6.42
0.245	-26.11	-16.11	-6.11
0.262	-25.82	-15.82	-5.82
0.278	-25.55	-15.55	-5.55
0.295	-25.30	-15.30	-5.30
0.312	-25.06	-15.06	-5.06
0.329	-24.83	-14.83	-4.83
0.346	-24.61	-14.61	-4.61
0.362	-24.41	-14.41	-4.41
0.379	-24.21	-14.21	-4.21
0.396	-24.02	-14.02	-4.02
0.413	-23.84	-13.84	-3.84
0.429	-23.67	-13.67	-3.67
0.446	-23.50	-13.50	-3.50
0.463	-23.34	-13.34	-3.34
0.480	-23.19	-13.19	-3.19
0.497	-23.04	-13.04	-3.04

Page 2	Range		
	100mV / uW	10mV / uW	1mV / uW
Output Voltage	DBM	DBM	DBM
0.513	-22.90	-12.90	-2.90
0.530	-22.76	-12.76	-2.76
0.547	-22.62	-12.62	-2.62
0.564	-22.49	-12.49	-2.49
0.581	-22.36	-12.36	-2.36
0.597	-22.24	-12.24	-2.24
0.614	-22.12	-12.12	-2.12
0.631	-22.00	-12.00	-2.00
0.648	-21.89	-11.89	-1.89
0.664	-21.78	-11.78	-1.78
0.681	-21.67	-11.67	-1.67
0.698	-21.56	-11.56	-1.56
0.715	-21.46	-11.46	-1.46
0.732	-21.36	-11.36	-1.36
0.748	-21.26	-11.26	-1.26
0.765	-21.16	-11.16	-1.16
0.782	-21.07	-11.07	-1.07
0.799	-20.98	-10.98	-0.98
0.815	-20.89	-10.89	-0.89
0.832	-20.80	-10.80	-0.80
0.849	-20.71	-10.71	-0.71
0.866	-20.63	-10.63	-0.63
0.883	-20.54	-10.54	-0.54
0.899	-20.46	-10.46	-0.46
0.916	-20.38	-10.38	-0.38
0.933	-20.30	-10.30	-0.30
0.950	-20.22	-10.22	-0.22
0.966	-20.15	-10.15	-0.15
0.983	-20.07	-10.07	-0.07
1.000	-20.00	-10.00	0.00

B. MEASURED SPLITTING LOSSES

The following is a summary of the actual losses measured from input lead to each output lead for each the 1 × 4 splitters used in this thesis.

	Measured losses (–dB)			
Device ID number	Output lead #1	Output lead #2	Output lead #3	Output lead #4
580	–7.0	–7.3	–7.1	–6.5
581	–7.1	–6.4	–6.1	–7.1
582	–7.4	–6.4	–6.1	–7.1
583	–6.3	–7.5	–6.7	–7.5
584	–6.8	–7.2	–6.2	–7.1
585	–7.6	–6.9	–6.9	–7.5
586	–7.7	–6.8	–6.9	–7.7
587	–6.3	–7.2	–6.9	–7.7

C. MATLAB SOURCE CODE

Source code and data file for MATLAB sorting program.

Splitt.dat - data file containing measured splitting losses.

```
**********************************************************************************************
6.5 7.0 7.1 7.3
6.3 6.8 7.4 7.4
6.1 6.4 7.1 7.4
6.3 6.7 7.5 7.5
6.2 6.8 7.1 7.2
6.9 6.9 7.5 7.6
6.8 6.9 7.7 7.7
6.3 6.9 7.2 7.7
```

RR.m - MATLAB function used to rotate right a row vector.

```
**********************************************************************************************
    function [x]=rr(y);
    l=length(y);
    z=zeros(1:l+1);
    x=zeros(1:l);
    z(2:l+1)=y;
    x(1)=z(l+1);
x(2:l)=z(2:l);
```

Splitt.m - MATLAB source code used to find optimum component combination.

```
**********************************************************************************************
clear
load splitt.dat;        * Load data file *
a=splitt;               * Assign data to matrix variable "a" *
clear splitt;           * Clear old variable *
b=[0.9 0.7 0.5 0.0];    * Assign delay line losses to vector  variable "b" *
S=2                     * Assign an inital standard deviation to variable "S" *

for l = 1:8             * Begin first loop through matrix*
 r1=a(l,:);             * Assign l^th row of matrix to variable "r1" *

 for m = 1:8            * Begin second loop through matrix*
  r2=a(m,:);            * Assign m^th row of matrix to variable "r2" *
```

```
if l ~= m           * Check for the same rows, bypass if equal *

 for i = 1:4        * Begin first loop through row vector r1*
  r1=rr(r1);        * Rotate right r1 *
  s=r1+r2+b;        * Sum up vectors *
  x=std(s);         * Take standard deviation of vector  *
  if x < S          * Test for lower value *
   S=x;             * Make assignments if true *
   ra1=r1;
   ra2=r2;
   ba=b;
  end

  for j = 1:4               * Begin second loop through row vector r2*
   r2=rr(r2);       * Rotate right r2 *
   s=r1+r2+b;       * Sum up vectors *
   x=std(s);        * Take standard deviation of vector *
   if x < S         * Test for lower value *
    S=x;            * Make assignments if true *
    ra1=r1;
    ra2=r2;
    ba=b;
   end

   for k = 1:4      * Begin third loop through row vector b*
    b=rr(b);        * Rotate right r2 *
    s=r1+r2+b;      * Sum up vectors *
    x=std(s);       * Take standard deviation of vector  *
    if x < S                * Test for lower value *
     S=x;           * Make assignments if true *
     ra1=r1;
     ra2=r2;
     ba=b;
    end
   end
  end
 end
end

S                   * Display results *
ra1
```

ra2
ba

********** End of Program**********

LIST OF REFERENCES

1. Couch II, L. W., *Digital and Analog Communication Systems*, 3rd ed., Macmillan Publishing Company, New York, 1990.

2. Rodger E. Ziemer and Roger L. Peterson, *Digital Communications and Spread Spectrum Sysyems*, Macmillan Publishing Company, New York, 1985.

3. Ha, T. T., *Digital Satellite Communications*, 2nd ed., McGraw-Hill Publishing Company, 1990.

4. Viterbi, A. J., "When Not to Spread Spectrum - A Sequel," *IEEE Communications Magazine*, vol. 23, April 1985, pp. 12-17.

5. J. A. Salehi and C. A. Bracket, "Fundamental Principles of Fiber Optic Code Division Multiple Access (FO-CDMA)," Proc. IEEE Int. Conf. Communications, Seattle, WA, pp. 1601-1609, 1987.

6. J. A. Salehi, "Code Division Multiple-User Techniques in Optical Fiber Networks -- Part I: Fundamental Principles," *IEEE Trans. Comm.*, vol. COM-37, no. 8, pp. 834-842, 1989.

7. S. Tamura, S. Nakano, and K. Akazaki, "Optical Code-Multiplex Transmission by Gold Sequences", *J. Lightwave Technol.*, vol. 3, no.2, pp. 121-127, 1985.

8. P. R Pruncal, M. A. Santoro, and T.R. Fan, "Spread Spectrum Fiber-Optic Local Area Network Using Optical Processing," *IEEE Journal of Lightwave Tech.*, vol. LT-4, no. 5, pp. 547-554, 1986.

9. Tracy Alan Fischer, Lieutenant, United States Navy, "Code Division Multiple Access Applied to Fiber Optic Data Transmission," Naval Postgraduate School, Monterey, California, MSEE Thesis, September, 1987.

10. Scott M. Sundt, Lieutenant, United States Navy, "Implementation of a Code Division Multiple Access Transmitter/Receiver Scheme Utilizing a Fiber Optic Medium," Naval Postgraduate School, Monterey, California, MSEE Thesis, December, 1987.

11. K. P. Jackson, S. A. Newton, B. Moslehi, M. Tur, C. C. Cutlter, J. W. Goodman, and H. J. Shaw, "Optical Fiber Delay-Line Signal Processing," *IEEE Trans. Microwave Theory Tech.*, vol. MTT-33, no. 3, pp. 193-210, 1985.

12. F.R.K. Chung, J. A. Salehi, and V.K. Wei, "Optical Orthogonal Codes: Design, Analysis and Applications," *IEEE Trans. Info Theory*, vol. IT-35, no. 3, pp. 595-604, 1989.

13. Farhad Khansefid, Robert Gagliardi, and Herbert Taylor, "Design of (0,1) Sequences for Pulsed Coded Systems," Prepublication manuscript submitted May 7, 1990 to *IEEE Trans. Comm.*

14. Gerd Keiser, *Optical Fiber Communicationss*, 2nd ed., McGraw-Hill, Inc, New York, 1991.

15. Textronix, *RTD 720A Transient Digitizer*, User Manual, Textronix Inc., 1992.

16. Photodyne, *Model 1600XP Waveform Analyzer*, Instruction Manual, Photodyne Inc., 1982.

17. Charles W. Therrien, *Discrete Random Signals and Statistical Signal Processing*, manuscript, Naval Postgraduate School, Montery, California, 18 March, 1991.

INITIAL DISTRIBUTION LIST

		No. Copies
1.	Defense Technical Information Center Cameron Station Alexandria, Virginia 22304-6145	2
2.	Dudley Knox Library, Code 52 Naval Postgraduate School Monterey, California 93943-5002	2
3.	Chairman, Code EC Department of Electrical and Computer Engineering Naval Postgraduate School Monterey, California 93943-5002	1
4.	Professor John P. Powers, Code EC/Po Department of Electrical and Computer Engineering Naval Postgraduate School Monterey, California 93943-5002	2
5.	Professor Alex W. Lam, Code EC/La Department of Electrical and Computer Engineering Naval Postgraduate School Monterey, California 93943-5002	1
6.	Commander Naval Command, Control and Ocean Surveillance Center RDT&E Division Attn: A. Nakagawa, Code 425 San Diego, California 92151-5000	1
7.	Commander Naval Command, Control and Ocean Surveillance Center RDT&E Division Attn: N. Kamikawa, Code 534H San Diego, California 92151-5000	1

No. Copies

8. Commander 1
Naval Command, Control and Ocean Surveillance Center
RDT&E Division
Attn: M. Brininstool, Code 946
San Diego, California 92151-5000

9. Lieutenant John W. Andre, USN 1
16 Oak Ave
Riverside, Rhode Island 02915